Chapter 7

Showing the Similarity Between Cu^{II} μ-Oxo and Cu^{II} μ-Thiolate species by Catalytic Catechol Oxidation

A large library of Cu^{II} complexes with mononucleating and dinucleating ligands was synthesized to investigate their potential as catalysts for the catalytic oxidation of 3,5-di-tert-butylcatechol (3,5-DTBC). X-ray structure determination of a number of these complexes revealed relatively large Cu…Cu distances and the formation of polymeric species. Comparison of the 3,5-DTBC oxidation rates showed that the ligands that stabilize the biomimetic dinuclear Cu^{II} μ-thiolate complex also result in copper compounds that are much more active in the oxidation of 3,5-DTBC. The activity is inhibited by the presence of chloride ions. The highest turnover frequency that was observed was 7800 h^{-1}, which is one of the highest turnover frequencies for catechol oxidation in CH_3CN. These results demonstrate the similarities between the copper-thiolate and copper-oxygen chemistry.

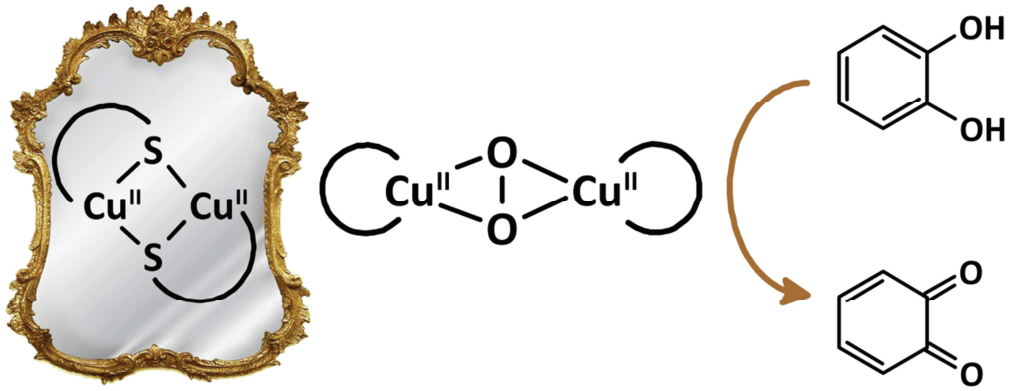

This chapter will be published as a full paper: E. C. M. Ording-Wenker, M. A. Siegler, M. Lutz, E. Bouwman, *submitted for publication*.

7.1 Introduction

The formation and redox properties of synthetic dinuclear Cu^{II} μ-thiolate complexes have been investigated because of their similarity to the Cu_A site (Section 1.3). It was found that small changes in the ligand structure can direct the reaction with copper salts towards the formation of either a Cu^{II} μ-thiolate or a Cu^{I} disulfide complex and that these species can inter-convert (Chapter 2).[1, 2] In Chapter 6 it is shown that this type of complexes exhibits redox chemistry with phenolates that is similar to that with thiolates, indicating that the oxygen chemistry might be very similar to the sulfur chemistry. This is also indicated by the fact that changes in the ligand structure similar to those that influence the Cu^{II} μ-thiolate/Cu^{I} disulfide equilibrium can induce a difference in coordination mode of dioxygen to copper.[3, 4] Additionally, the redox conversion of a Cu^{II}_2 μ-η^2:η^2-peroxide complex into a Cu^{III}_2 (μ-oxo)$_2$ species is reported.[5] To test whether copper-thiolate chemistry is similar to copper-oxygen chemistry the biomimetic catalytic oxidation of 3,5-di-*tert*-butylcatechol (3,5-DTBC) to 3,5-di-*tert*-butyl-*o*-benzoquinone (3,5-DTBQ) was investigated. The oxidation of catechol to quinone by catechol oxidase is thought to go *via* a Cu^{II}_2 μ-η^2:η^2-peroxide species (Section 1.2.3)[6-8] that shows similarities to the Cu^{II} μ-thiolate complex (Figure 7.1), although involvement of other types of Cu_2O_2 intermediates cannot be ruled out.[9] The oxidation of 3,5-DTBC is easy to monitor and is used as a common test reaction for new biomimetic copper complexes.[8] The structural and electronic similarity between the Cu^{II} μ-thiolate and Cu^{II}_2 μ-η^2:η^2-peroxide complex might lead to a more effective or more stabilizing reaction with O_2 by complexes of ligands that promote Cu^{II} μ-thiolate formation. Although it must be noted that if a Cu^{II} μ-thiolate species would form, it might be oxygenated by dioxygen (Chapter 4).[10]

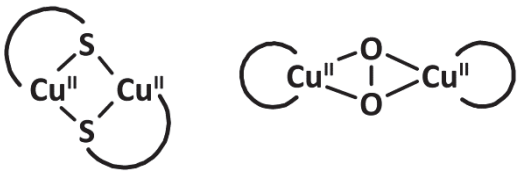

Figure 7.1: Schematic representation of a Cu^{II} μ-thiolate species and a side-on Cu^{II}_2 μ-η^2:η^2-peroxide species showing their similarity.

In this chapter the synthesis of a series of Cu^{II} complexes with mononucleating and dinucleating ligands is described. To have a complete picture of the effect of small ligand changes on the catechol oxidation activity, a large library of ligands was

rationally selected for this study (Figure 7.2). X-ray crystal structures were obtained for a number of the copper complexes and some of these will be discussed.

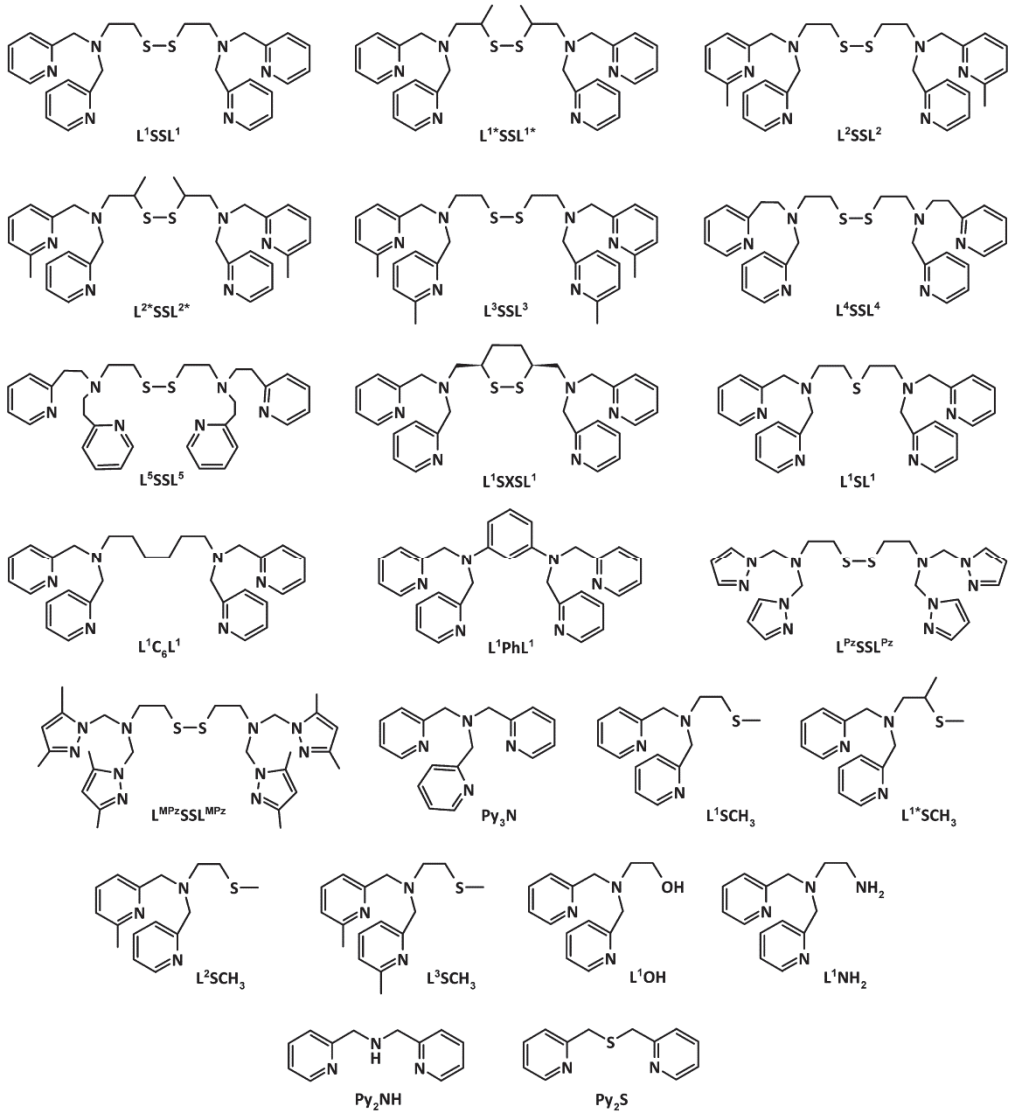

Figure 7.2: Schematic overview of the ligands that were synthesized for the study of the copper-catalyzed oxidation of catechol.

7.2 Results

7.2.1 Ligand and Complex Synthesis

Most of the ligands shown in Figure 7.2 were synthesized according to literature procedures (Chapter 2, 5 and 6)[1, 2, 11-16] or are commercially available. As the ligands are similar to each other, they were systematically named by their structure. For example **L**^{1} stands for the fragment *N*,*N*-bis(2-pyridylmethyl)aminoethyl and **Py** for 2-pyridylmethyl. Four new ligands were synthesized: **L**^{1}**SL**^{1}, **L**^{1}***SCH**$_3$, **L**^{2}**SCH**$_3$ and **L**^{3}**SCH**$_3$. **L**^{1}**SL**^{1} was synthesized by reductive amination of 1,5-diamino-3-thiapentane dihydrobromide, which was made via a 4-step literature procedure.[17] The complete synthesis scheme is depicted in Figure 7.3. Ligand **L**^{1}**SL**^{1} was obtained in 68% yield as a brown oil that turns darker over time. The ligand is not stable and slowly degrades over weeks even when kept under argon at 0 °C. When **L**^{1}**SL**^{1} is coordinated to copper, the complex does not degrade over time.

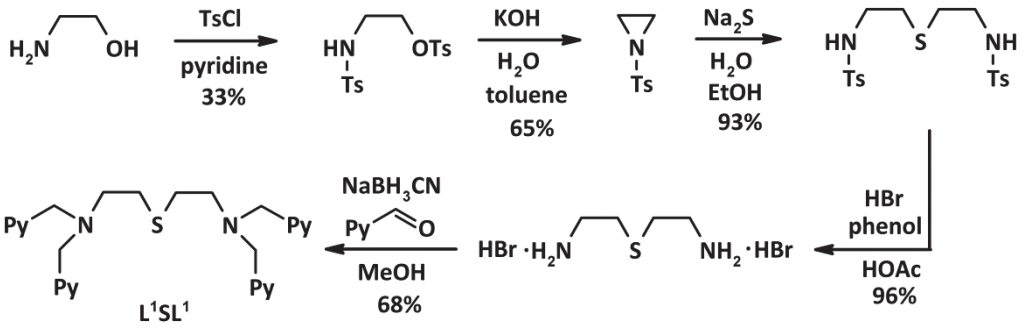

Figure 7.3: Synthesis scheme for **L**^{1}**SL**^{1}.[17] Abbreviations: Ts = 4-toluenesulfonyl; Ac = acetyl; Py = 2-pyridyl.

L^{1}***SCH**$_3$ was synthesized by reaction of propylene sulfide with di-(2-pyridylmethyl)amine in acetonitrile. After solvent evaporation, tetrahydrofuran and NaH were added to deprotonate the thiol. Addition of CH_3I yields **L**^{1}***SCH**$_3$, which was purified by column chromatography, resulting in 86% yield. **L**^{2}**SCH**$_3$ and **L**^{3}**SCH**$_3$ were obtained in relatively moderate yields of 50% and 46% by a two-step reductive amination using $NaBH_4$. The synthesis scheme for **L**^{1}***SCH**$_3$, **L**^{2}**SCH**$_3$ and **L**^{3}**SCH**$_3$ is shown in Figure 7.4. Like **L**^{1}**SL**^{1}, all three ligands degrade over time as indicated by darkening of the oil. The ligand **Py**$_2$**S** has been reported,[18] but its synthesis has not been described elaborately, which is why it is described in Section 7.5.3. **L**^{1}**OH** has also been reported,[19] but a slightly different method has been developed giving an almost quantitative yield of 99%.

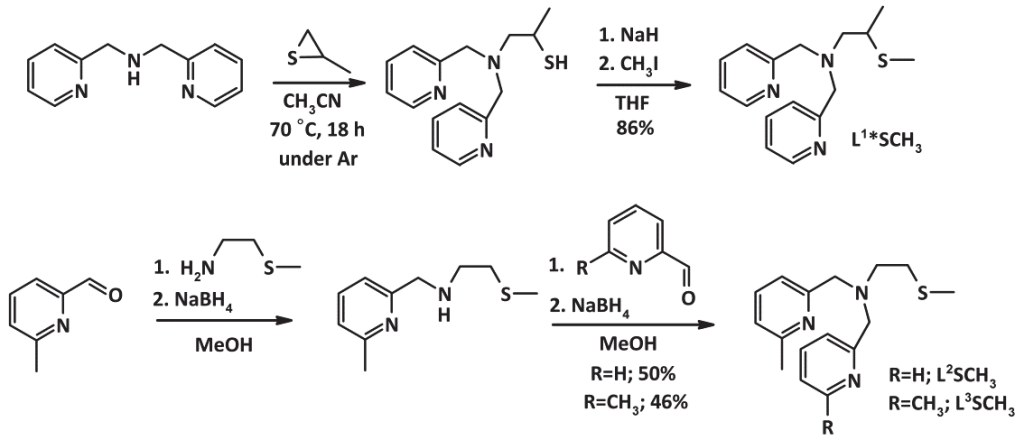

Figure 7.4: Synthesis scheme for $\mathbf{L^1{*}SCH_3}$, $\mathbf{L^2SCH_3}$ and $\mathbf{L^3SCH_3}$. Abbreviation THF = tetrahydrofuran.

With the 22 ligands that were either bought or synthesized, Cu^{II} complexes were formed with one Cl^- and one BF_4^- counterion per copper center. The general synthesis of these complexes entails the addition of a 1:1 mixture of $[Cu^{II}(H_2O)_6](BF_4)_2$ and $Cu^{II}Cl_2 \cdot 2\ H_2O$ to the ligand dissolved in methanol, or in the case of $\mathbf{L^2SSL^2}$ and $\mathbf{L^1NH_2}$ in CH_3CN. If the complex did not precipitate spontaneously, precipitation was induced by addition of diethyl ether. Copper compounds of ligands that can potentially form dinuclear complexes are more likely to form polymeric structures (see Section 7.2.2 and Chapter 5) and are tentatively given the formula: $[Cu^{II}_2(ligand)(Cl)_2]_n(BF_2)_n$. The complexes of ligands that are expected to form mononuclear compounds are indicated with the formula $[Cu^{II}(ligand)(Cl)](BF_4)$.

A copper complex with $\mathbf{L^5SSL^5}$ could not be isolated as a solid; all attempts resulted in the formation of oil. For the catalytic experiments (Section 7.2.3), this complex was formed in situ. In the synthesis of a complex with $\mathbf{L^2SSL^2}$, $[Cu^{II}(H_2O)_6](ClO_4)_2$ was used instead of $[Cu^{II}(H_2O)_6](BF_4)_2$ to grow single crystals suitable for X-ray structure diffraction. However, the complex $[Cu^{II}_2(\mathbf{L^2SSL^2})(Cl)_2]_n(BF_4)_{2n}$ was also synthesized, so that all catalysts used for catechol oxidation have the same counterions.

With the ligand $\mathbf{L^1{*}SCH_3}$ two complexes were formed: $[Cu^{II}(\mathbf{L^1{*}SCH_3})(Cl)]_2(CuCl_4)$ and $[Cu^{II}(\mathbf{L^1{*}SCH_3})(Cl)](BF_4)$. The first compound was obtained by addition of 1 equiv of $Cu^{II}Cl_2 \cdot 2\ H_2O$ to $\mathbf{L^1{*}SCH_3}$, the latter from 0.5 equiv of $Cu^{II}Cl_2 \cdot 2\ H_2O$ and 0.5 equiv. of $[Cu^{II}(H_2O)_6](BF_4)_2$. The X-ray crystal structures were determined of both complexes and the structures of their cationic copper complex were found to be very

similar. Appendix VI contains the crystallographic information for both these structures.

The UV-vis spectra of all the Cu^{II} complexes are highly similar, showing LMCT bands of $Cu^{II} \leftarrow S$ and $Cu^{II} \leftarrow Cl$ in the region between 200 and 400 nm and one or two bands in the range of 650 to 940 nm that can be ascribed to Cu^{II} d-d transitions (Appendix VI, Figure AVI.3).

7.2.2 Description of X-ray Crystal Structures

Single crystals could be obtained for several of the synthesized Cu^{II} complexes. This led to the X-ray crystal structure determination of the polymeric complexes $[Cu^{II}_2(\mathbf{L^1SSL^1})(Cl)_2]_n(BF_4)_{2n}$, $[Cu^{II}_2(\mathbf{L^2SSL^2})(Cl)_2]_n(ClO_4)_{2n}$, $[Cu^{II}_2(\mathbf{L^1SL^1})(Cl)_2]_n(BF_4)_{2n}$ and $[Cu^{II}_2(\mathbf{L^1C_6L^1})(Cl)_2]_n(BF_4)_{2n}$ and of the compounds of mononucleating ligands, namely $[Cu^{II}(\mathbf{L^1{*}SCH_3})(Cl)](BF_4)$, $[Cu^{II}(\mathbf{L^1{*}SCH_3})(Cl)]_2(CuCl_4)$, $[Cu^{II}(\mathbf{L^2SCH_3})(Cl)](BF_4)$, $[Cu^{II}(\mathbf{L^3SCH_3})(Cl)](BF_4)$ and $[Cu^{II}(\mathbf{L^1NH_2})(Cl)](BF_4)$. The copper ions in the polymeric structures $[Cu^{II}_2(\mathbf{L^1SSL^1})(Cl)_2]_n(BF_4)_{2n}$, $[Cu^{II}_2(\mathbf{L^2SSL^2})(Cl)_2]_n(ClO_4)_{2n}$ and $[Cu^{II}_2(\mathbf{L^1SL^1})(Cl)_2]_n(BF_4)_{2n}$ have very similar coordination geometries; $[Cu^{II}_2(\mathbf{L^1SSL^1})(Cl)_2]_n(BF_4)_{2n}$ and $[Cu^{II}_2(\mathbf{L^2SSL^2})(Cl)_2]_n(ClO_4)_{2n}$ will not be discussed, but crystallographic data and selected bond distances and angles can be found in Appendix VI. Similarly the structures of $[Cu^{II}(\mathbf{L^1{*}SCH_3})(Cl)](BF_4)$ and $[Cu^{II}(\mathbf{L^1{*}SCH_3})(Cl)]_2(CuCl_4)$ are comparable to that of $[Cu^{II}(\mathbf{L^2SCH_3})(Cl)](BF_4)$ and information concerning these structures can be found in Appendix VI.

Thus, the structures of $[Cu^{II}_2(\mathbf{L^1SL^1})(Cl)_2]_n(BF_4)_{2n}$, $[Cu^{II}_2(\mathbf{L^1C_6L^1})(Cl)_2]_n(BF_4)_{2n}$, $[Cu^{II}(\mathbf{L^2SCH_3})(Cl)](BF_4)$, $[Cu^{II}(\mathbf{L^3SCH_3})(Cl)](BF_4)$ and $[Cu^{II}(\mathbf{L^1NH_2})(Cl)](BF_4)$ are described. The crystallographic and structure refinement data for these complexes are collected in Table 7.1.

Single crystals of $[Cu^{II}_2(\mathbf{L^1SL^1})(Cl)_2]_n(BF_4)_{2n}$ were obtained by slow evaporation of diethyl ether into a solution of the complex in acetonitrile. A displacement ellipsoid plot of $[Cu^{II}_2(\mathbf{L^1SL^1})(Cl)_2]_n(BF_4)_{2n}$ is shown in Figure 7.5 and selected bond distances and angles are provided in Table 7.2. $[Cu^{II}_2(\mathbf{L^1SL^1})(Cl)_2]_n(BF_4)_{2n}$ crystallizes in the monoclinic space group *C*2/*c*, with half a dinuclear compound and one BF_4^- ion in the asymmetric unit. The structure is very disordered. Both the Cu complex and the BF_4^- counterions are found to be disordered over two orientations. The major and minor components of the Cu complex are related by a pseudo-mirror plane, and the occupancy factor of the major component of the disorder refines to 0.840(3). Both counterions are found at sites of twofold axial symmetry, and are constrained to be disordered with an occupancy factor of 0.5.

Table 7.1: Crystallographic and structure refinement data for complex $[Cu^{II}_2(\mathbf{L^1SL^1})(Cl)_2]_n(BF_4)_{2n}$, $[Cu^{II}_2(\mathbf{L^1C_6L^1})(Cl)_2]_n(BF_4)_{2n}$, $[Cu^{II}(\mathbf{L^2SCH_3})(Cl)](BF_4)$, $[Cu^{II}(\mathbf{L^3SCH_3})(Cl)](BF_4)$ and $[Cu^{II}(\mathbf{L^1NH_2})(Cl)](BF_4)$.

	$[Cu^{II}_2(\mathbf{L^1SL^1})(Cl)_2]_n(BF_4)_{2n}$	$[Cu^{II}_2(\mathbf{L^1C_6L^1})(Cl)_2]_n(BF_4)_{2n}$	$[Cu^{II}(\mathbf{L^2SCH_3})(Cl)](BF_4)$	$[Cu^{II}(\mathbf{L^3SCH_3})(Cl)](BF_4)$	$[Cu^{II}(\mathbf{L^1NH_2})(Cl)](BF_4)$
empirical formula	$[C_{28}H_{32}Cl_2Cu_2N_6S](BF_4)_2$	$[C_{30}H_{36}Cl_2Cu_2N_6](BF_4)_2 \cdot 4\ CH_3CN$	$[C_{16}H_{21}ClCuN_3S](BF_4)$	$[C_{17}H_{23}ClCuN_3S](BF_4)$	$[C_{14}H_{18}ClCuN_4](BF_4)$
formula weight	856.25	1016.46	473.22	487.24	428.12
crystal system	monoclinic	monoclinic	monoclinic	monoclinic	monoclinic
space group	$C2/c$	$C2/m$	$C2/m$	$P2_1/c$	$P2_1/n$
a, Å	10.0603(8)	13.287(2)	13.0671(3)	9.11412(10)	8.92176(15)
b, Å	23.2653(15)	27.558(5)	20.2293(5)	15.17627(13)	12.8949(3)
c, Å	14.5686(9)	6.9232(17)	7.40187(15)	15.31060(15)	14.9606(3)
β, deg	100.321(7)	111.421(13)	101.660(2)	102.6105(10)	102.0565(19)
V, Å^3	3354.7(4)	2359.9(8)	1916.22(8)	2066.65(4)	1683.18(6)
Z	4	2	4	4	4
D_{calc}, g·cm^3	1.695	1.430	1.640	1.566	1.689
T, Kelvin	110(2)	150(2)	110(2)	110(2)	110(2)
crystal size, mm	$0.43 \times 0.14 \times 0.08$	$0.30 \times 0.30 \times 0.30$	$0.35 \times 0.28 \times 0.20$	$0.40 \times 0.32 \times 0.22$	$0.50 \times 0.36 \times 0.14$
μ, mm^{-1}	1.566	1.085	4.318	4.021	1.502
no. of reflns measd	9412	9970	6657	14162	13962
no. of unique reflns	2953	1904	1913	4035	3879
no. of reflns obsd.	2550 [$I > 2\sigma(I)$]	1601 [$I > 2\sigma(I)$]	1791 [$I > 2\sigma(I)$]	3893 [$I > 2\sigma(I)$]	3414 [$I > 2\sigma(I)$]
no. of parameters	444	172	246	303	234
R_1 / wR_2 [$I > 2\sigma(I)$]	0.0538/0.1394	0.0780/0.2007	0.0327/0.0861	0.0240/0.0635	0.0257/0.0675
R_1 / wR_2 [all refl.]	0.0621/0.1452	0.0942/0.2123	0.0346/0.0879	0.0250/0.0641	0.0305/0.0693
goodness of fit	1.029	1.151	1.046	1.054	1.080
$\Delta\rho$, e·Å^{-3}	−0.57/0.81	-1.22/1.04	−0.24/0.45	−0.30/0.39	−0.48/0.31

Table 7.2: Selected bond distances (Å) and bond angles (°) for complexes $[Cu^{II}_2(\mathbf{L^1SL^1})(Cl)_2]_n(BF_4)_{2n}$ and $[Cu^{II}_2(\mathbf{L^1C_6L^1})(Cl)_2]_n(BF_4)_{2n}$.

	$[Cu^{II}_2(\mathbf{L^1SL^1})(Cl)_2]_n(BF_4)_{2n}$	$[Cu^{II}_2(\mathbf{L^1C_6L^1})(Cl)_2]_n(BF_4)_{2n}$
Cu1 - Cu1*	3.6986(7)	3.405(2)
Cu1 - Cu1#	5.0511(7)	12.013(3)
Cu1 - S1	2.6825(7)	
Cu1 - N1	2.057(4)	2.026(9)
Cu1 - N11	2.004(4)	1.987(6)
Cu1 - N21/N11'	1.987(4)	1.987(6)
Cu1 - Cl1	2.278(2)	2.223(3)
Cu1 - Cl1*	2.879(2)	2.865(4)
S1 - Cu1 - N1	84.72(12)	
S1 - Cu1 - N11	83.29(11)	
S1 - Cu1 - N21	100.27(11)	
S1 - Cu1 - Cl1*	166.13(5)	
N1 - Cu1 - N11	82.77(18)	82.88(18)
N1 - Cu1 - N21/N11'	80.87(17)	82.88(18)
N1 - Cu1 - Cl1	177.93(13)	173.7(3)
N11 - Cu1 - N21/N11'	162.84(18)	165.5(4)

Symmetry operation * = [1–x, –y, –z] and # = [1–x, y, ½–z] for $[Cu^{II}_2(\mathbf{L^1SL^1})(Cl)_2]_n(BF_4)_{2n}$; Symmetry operation * = [1–x, y, 1–z]; # = [–x, y, –1–z]; ' = [x, –y, z] for $[Cu^{II}_2(\mathbf{L^1C_6L^1})(Cl)_2]_n(BF_4)_{2n}$.

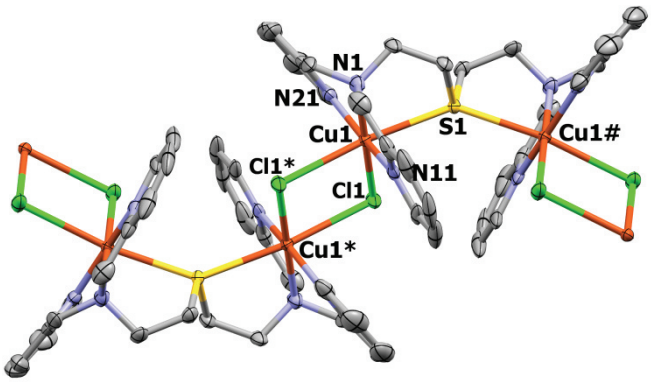

Figure 7.5: Displacement ellipsoid plot (50% probability level) of two of the repeating units in the cationic polymer chain of $[Cu^{II}_2(\mathbf{L^1SL^1})(Cl)_2]_n(BF_4)_{2n}$. The disorder, the non-coordinating counterions and hydrogen atoms are omitted for clarity. Symmetry operation * = [1–x, –y, –z] and # = [1–x, y, ½–z].

The thioether sulfur atom of the dinucleating ligand bridges between the two copper ions, resulting in a distorted octahedral N_3SCl_2 coordination environment for both copper ions. The elongated Jahn-Teller axis is occupied by S1 and Cl1* (Cu1-S1

2.6825(7) Å; Cu1-Cl1* 2.879(2) Å). The chloride ions are bridging between copper ions of neighboring dinuclear complexes resulting in infinite 1D zig-zag chains. The distance between the copper ions in the Cu(μ-Cl)$_2$Cu core is 3.6986(7) Å. This distance is slightly larger than the Cu…Cu distances in [Cu$^{II}_2$(**L^{1}SSL^1**)(Cl)$_2$]$_n$(BF$_4$)$_{2n}$ and [Cu$^{II}_2$(**L^{2}SSL^2**)(Cl)$_2$]$_n$(BF$_4$)$_{2n}$, which are ca. 3.60 Å (average) and 3.6455(4) Å, respectively (Appendix VI, Table AVI.2).

[Cu$^{II}_2$(**L^{1}C$_6$L^1**)(Cl)$_2$]$_n$(BF$_4$)$_{2n}$ · 4 CH$_3$CN crystallized from acetonitrile and di-isopropyl ether. The metal and chloride ions and the 1,6-diaminohexane backbone are lying in a mirror plane and in addition the molecule contains two-fold rotational symmetry; the BF$_4^-$ anion is disordered on a twofold axis, and the acetonitrile molecule is located on a general position. The asymmetric unit consequently contains ¼ of the ligand, half a copper center, half a Cl$^-$ ion, half a BF$_4^-$ ion and one CH$_3$CN molecule. A displacement ellipsoid plot is shown in Figure 7.6a. Selected bond distances and angles can be found in Table 7.2. The copper ions in [Cu$^{II}_2$(**L^{1}C$_6$L^1**)(Cl)$_2$]$_n$(BF$_4$)$_{2n}$ are in an N$_3$Cl$_2$ coordination environment, in a distorted square-pyramidal geometry that resembles that of the copper ions in [Cu$^{II}_2$(**L^{1}SL^1**)(Cl)$_2$]$_n$(BF$_4$)$_{2n}$, except for the coordination of a sulfur atom. The chloride ions are bridging between copper ions of neighboring dinuclear complexes resulting in infinite linear 1D chains. The Cu1-Cu1* distance in the Cu(μ-Cl)$_2$Cu core is 3.405(2) Å, which is significantly smaller than in sulfur-containing complexes such as [Cu$^{II}_2$(**L^{1}SL^1**)(Cl)$_2$]$_n$(BF$_4$)$_{2n}$. The structure of the related dinuclear complex [Cu$^{II}_2$(**L^{1}C$_6$L^1**)(Cl)$_4$], which does not form polymeric structures, was recently reported;[20] the copper ions in the two structures have very similar coordination geometries (Figure 7.6b).

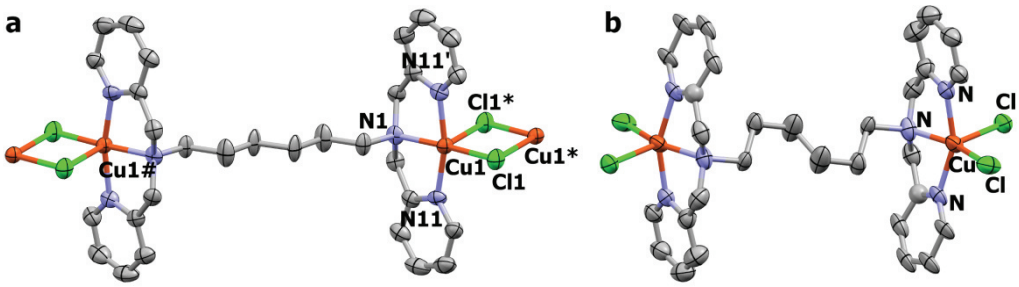

Figure 7.6: Displacement ellipsoid plots (50% probability level) of (a) the cationic part of [Cu$^{II}_2$(**L^{1}C$_6$L^1**)(Cl)$_2$]$_n$(BF$_4$)$_{2n}$ and (b) [Cu$^{II}_2$(**L^{1}C$_6$L^1**)(Cl)$_4$].[20] Non-coordinating counterions and hydrogen atoms are omitted for clarity. Symmetry operation * = [1–x, y, 1–z]; # = [–x, y, –1–z]; ' = [x, –y, z].

The major difference between the structures is that the hexamethylene bridge in $[Cu^{II}_2(\mathbf{L^1C_6L^1})(Cl)_4]$ has a crystallographic C_{2h} symmetry and forms an 'alternating' chain whereas in $[Cu^{II}_2(\mathbf{L^1C_6L^1})(Cl)_2]_n(BF_4)_{2n}$ it forms a linear chain, which is the expected, thermodynamically favored conformation.

The three compounds $[Cu^{II}(\mathbf{L^2SCH_3})(Cl)](BF_4)$, $[Cu^{II}(\mathbf{L^3SCH_3})(Cl)](BF_4)$ and $[Cu^{II}(\mathbf{L^1NH_2})(Cl)](BF_4)$ all crystallized in structures with one mononuclear complex and one BF_4^- counterion in the asymmetric unit. Displacement ellipsoid plots and selected bond distances and angles are given in Figure 7.7 and Table 7.3.

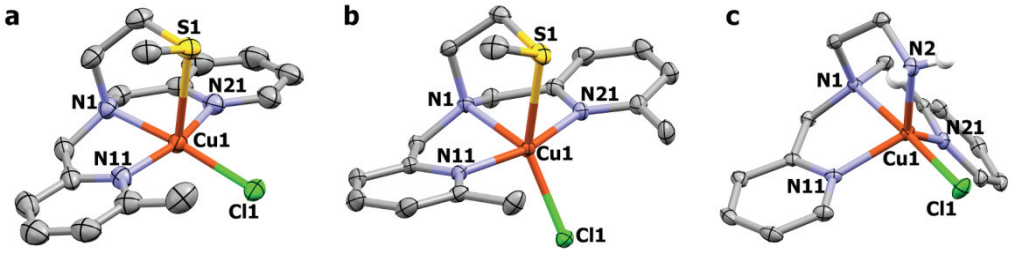

Figure 7.7: Displacement ellipsoid plots (50% probability level) of the cationic parts of (a) $[Cu^{II}(\mathbf{L^2SCH_3})(Cl)](BF_4)$, (b) $[Cu^{II}(\mathbf{L^3SCH_3})(Cl)](BF_4)$ and (c) $[Cu^{II}(\mathbf{L^1NH_2})(Cl)](BF_4)$. The disorder, the non-coordinating counterions and most of the hydrogen atoms are omitted for clarity.

$[Cu^{II}(\mathbf{L^2SCH_3})(Cl)](BF_4)$ crystallizes in the monoclinic space group *C*2/*m*. The copper complex and the BF_4^- counterion are found at sites of mirror and twofold rotation symmetry, respectively. As the complex cation has no mirror symmetry, it is disordered over two orientations with equal occupancy factors (*i.e.*, 0.5 for each component). The BF_4^- counterion is also found to be disordered over two orientations with equal occupancy factors. The copper ion has square-pyramidal geometry (τ = 0.12),[21] but forms a dimer via bridging chloride ions with another cationic subunit, thus creating an octahedral environment with Cl1* and S1 on the elongated Jahn-Teller axis (Cu1-S1 2.7260(9) Å; Cu1-Cl1* 2.9837(9) Å). The Cu1-Cu1* distance of 3.8504(5) Å is larger than in the polymeric species discussed above. Such formation of dimeric structures is also observed for $[Cu^{II}(\mathbf{L^1SCH_3})(Cl)](BF_4)$ (Chapter 6) and $[Cu^{II}(\mathbf{L^{1*}SCH_3})(Cl)](BF_4)$ (Appendix VI, Figure AVI.2).

The compounds $[Cu^{II}(\mathbf{L^3SCH_3})(Cl)](BF_4)$ and $[Cu^{II}(\mathbf{L^1NH_2})(Cl)](BF_4)$ crystallize in monoclinic space groups $P2_1/c$ and $P2_1/n$, respectively. These complexes do not form dimeric species, as their coordination geometry is more distorted towards trigonal bipyramidal with τ parameters of 0.39 and 0.84, respectively.

Table 7.3: Selected bond distances (Å) and bond angles (°) for complexes $[Cu^{II}(\mathbf{L^2SCH_3})(Cl)](BF_4)$, $[Cu^{II}(\mathbf{L^3SCH_3})(Cl)](BF_4)$ and $[Cu^{II}(\mathbf{L^1NH_2})(Cl)](BF_4)$.

	$[Cu^{II}(\mathbf{L^2SCH_3})(Cl)](BF_4)$	$[Cu^{II}(\mathbf{L^3SCH_3})(Cl)](BF_4)$	$[Cu^{II}(\mathbf{L^1NH_2})(Cl)](BF_4)$
Cu1 - Cu1*	3.8504(5)		
Cu1 - S1/N2	2.7260(9)	2.5817(4)	2.0593(15)
Cu1 - N1	2.048(3)	2.0876(12)	2.0439(12)
Cu1 - N11	2.046(5)	1.9914(12)	2.1158(13)
Cu1 - N21	2.002(5)	1.9935(13)	2.0410(13)
Cu1 - Cl1	2.2586(8)	2.2674(4)	2.2381(4)
Cu1 - Cl1*	2.9837(9)		
S1/N2 - Cu1 - N1	86.62(8)	85.75(3)	84.73(5)
S1/N2 - Cu1 - N11	94.7(2)	93.86(4)	109.75(6)
S1/N2 - Cu1 - N21	89.2(2)	82.92(4)	127.21(6)
S1/N2 - Cu1 - Cl1	102.38(3)	141.526(16)	96.44(4)
N1 - Cu1 - N11	80.6(3)	82.13(5)	80.25(5)
N1 - Cu1 - N21	83.4(3)	83.00(5)	81.87(5)
N1 - Cu1 - Cl1	170.52(12)	132.50(4)	177.49(4)
N11 - Cu1 - N21	163.28(15)	164.98(5)	117.72(5)
N11 - Cu1 - Cl1	101.3(2)	95.44(4)	97.26(4)
N21 - Cu1 - Cl1	93.7(2)	96.15(4)	99.12(4)

Symmetry operation * = [x, y, –1+z]

A structure similar to $[Cu^{II}(\mathbf{L^1NH_2})(Cl)](BF_4)$ has been reported in the literature with ClO_4^- instead of BF_4^- as the non-coordinating counterion; the copper ions in the two structures have the same trigonal-bipyramidal coordination geometry with the Cl^- ion and the tertiary nitrogen atom occupying the axial coordination sites.[22] In $[Cu^{II}(\mathbf{L^3SCH_3})(Cl)](BF_4)$ the axial positions are occupied by the pyridyl nitrogens.

7.2.3 Catechol oxidation

The synthesized complexes were tested for their catalytic activity in the oxidation of 3,5-DTBC to 3,5-DTBQ. The rate of oxidation was determined by monitoring the absorbance of 3,5-DTBQ at 400 nm. All catalytic experiments were conducted at 25 °C whilst stirring and bubbling a mixture of N_2 and O_2 (1:1) through the solution. A copper concentration of 0.4 mM, corresponding with 0.4 mM of a mononuclear complex or 0.2 mM of a dinuclear complex, was used together with 20 mM 3,5-DTBC. Upon addition of 20 mM NEt_3 the conversion of 3,5-DTBC started. The results of the catalytic experiments are collected in Table 7.4. Three different types of conversion curves were observed (A, B and C; Figure 7.8). Depending on the type of catalyst the oxidation rate was constant, increasing, or decreasing over time. For this reason both the maximum turnover frequencies (TOFs) and initial TOFs are reported in Table 7.4.

After addition of NEt_3, an abrupt increase in the absorption at 400 nm was observed for all copper complexes with one Cl^- and one BF_4^- counterion (Figure 7.8). The height of this 'jump' was dependent on the catalyst used and appeared to be related to the presence of chloride ions (see below). The initial TOF was determined by taking the tangent of the curve of the first two seconds after the 'jump' in the absorption curve. Blank reactions were performed in the presence and absence of copper (entry 1-2, Table 7.4). The blank reaction with copper was performed using a 1:1 mixture in acetonitrile of $[Cu^{II}(H_2O)_6](BF_4)_2$ and $CuCl_2 \cdot 2\ H_2O$ from which most of the H_2O content was removed by addition of Na_2SO_4. The catalytic activity of the copper complexes with mononucleating ligands is not much higher than for the system containing just the copper salts (entry 2 and 16-24, Table 7.4).

Table 7.4: Turnover frequencies of the oxidation of 3,5-DTBC to 3,5-DTBQ catalyzed by copper complexes with different ligands.[a]

	Ligand	Catalyst	Graph type[c]	max TOF (h^{-1})[d]	initial TOF (h^{-1})
1	-	no catalyst	C	170	15
2	-	$[Cu^{II}(Cl)](BF_4)$[b]	C	450	180
3	**L^1SSL^1**	$[Cu^{II}_2(ligand)(Cl)_2]_n(BF_4)_{2n}$	A	-	2150
4	**L^1*SSL^1***	$[Cu^{II}_2(ligand)(Cl)_2]_n(BF_4)_{2n}$	A	-	4700
5	**L^2SSL^2**	$[Cu^{II}_2(ligand)(Cl)_2]_n(BF_4)_{2n}$	A	-	570
6	**L^2*SSL^2***	$[Cu^{II}_2(ligand)(Cl)_2]_n(BF_4)_{2n}$	A	-	1750
7	**L^3SSL^3**	$[Cu^{II}_2(ligand)(Cl)_2]_n(BF_4)_{2n}$	C	240	190
8	**L^4SSL^4**	$[Cu^{II}_2(ligand)(Cl)_2]_n(BF_4)_{2n}$	A	-	3200
9	**L^5SSL^5**	$[Cu^{II}_2(ligand)(Cl)_2]_n(BF_4)_{2n}$[b]	C	310	120
10	**L^1SXSL^1**	$[Cu^{II}_2(ligand)(Cl)_2]_n(BF_4)_{2n}$	C	430	330
11	**L^1SL^1**	$[Cu^{II}_2(ligand)(Cl)_2]_n(BF_4)_{2n}$	A	-	1800
12	**$L^1C_6L^1$**	$[Cu^{II}_2(ligand)(Cl)_2]_n(BF_4)_{2n}$	A	-	530
13	**L^1PhL^1**	$[Cu^{II}_2(ligand)(Cl)_2]_n(BF_4)_{2n}$	C	580	190
14	**$L^{Pz}SSL^{Pz}$**	$[Cu^{II}_2(ligand)(Cl)_2]_n(BF_4)_{2n}$	C	390	240
15	**$L^{MPz}SSL^{MPz}$**	$[Cu^{II}_2(ligand)(Cl)_2]_n(BF_4)_{2n}$	C	390	170
16	**Py_3N**	$[Cu^{II}(ligand)(Cl)](BF_4)$	A	-	600
17	**L^1SCH_3**	$[Cu^{II}(ligand)(Cl)](BF_4)$	A	-	760
18	**L^1*SCH_3**	$[Cu^{II}(ligand)(Cl)](BF_4)$	C	480	370
19	**L^2SCH_3**	$[Cu^{II}(ligand)(Cl)](BF_4)$	C	330	150
20	**L^3SCH_3**	$[Cu^{II}(ligand)(Cl)](BF_4)$	C	220	110
21	**L^1OH**	$[Cu^{II}(ligand)(Cl)](BF_4)$	B	-	430
22	**L^1NH_2**	$[Cu^{II}(ligand)(Cl)](BF_4)$	B	-	340
23	**Py_2NH**	$[Cu^{II}(ligand)(Cl)](BF_4)$	A	-	440
24	**Py_2S**	$[Cu^{II}(ligand)(Cl)](BF_4)$	C	390	160

[a] Reaction conditions: 0.4 mM [Cu], 20 mM 3,5-DTBC, 20 mM NEt_3 in 3 mL CH_3CN. TOFs were determined from the change in absorbance of 3,5-DTBQ at 400 nm.

[b] Complex was formed in situ.

[c] The three different types of graphs A, B and C are depicted in Figure 7.8.

[d] Only given when maximum TOF is higher than initial TOF (graph type C).

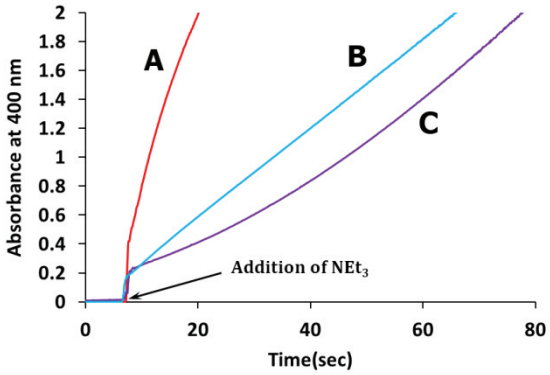

Figure 7.8: Development in time of the absorption at 400 nm due to 3,5-DTBQ formation, catalyzed by $[Cu^{II}_2(\mathbf{L^1SSL^1})(Cl)_2](BF_4)_2$ (red, type A), $[Cu^{II}(\mathbf{L^1OH})(Cl)](BF_4)$ (blue, type B) and $[Cu^{II}_2(\mathbf{L^{Pz}SSL^{Pz}})(Cl)_2](BF_4)_2$ (purple, type C).

In contrast, a number of the dinucleating ligands result in catalytic systems with significantly higher activity, which we will further elaborate on.

The catalytic system comprising the ligand $\mathbf{L^1SSL^1}$ shows reasonably high activity (entry 3), but introduction of methyl groups at the *ortho*-position of the pyridyl rings results in a considerable decrease of the catalytic activity (entry 3, 5 and 7). Addition of a methyl group next to the sulfur in the disulfide bond, however, results in significantly higher activity (entry 3-4, 5-6). Changing the bridge between the tertiary amine and the pyridyl groups from a methylene to an ethylene spacer at two positions leads to an increase in activity (entry 3 vs 8), but at four positions it leads to a dramatic decrease in activity (entry 3 vs 9). The use of pyridyl-containing ligands containing a disulfide bond generally results in higher TOFs, but the high catalytic activity of the system comprising $\mathbf{L^1SL^1}$ indicates that the presence of a thioether instead of a disulfide group can give similar performance (entry 3 vs 11). The presence of an S-donor atom in the ligand does have a positive effect on the catalytic activity of the system, considering that a similar complex with an alkane bridge ($\mathbf{L^1C_6L^1}$) shows a significantly lower TOF (entry 3 vs 12). The complex with ligand $\mathbf{L^1SXSL^1}$ has considerably lower activity than the compound with $\mathbf{L^{1*}SSL^{1*}}$, while these systems only differ in the rigidity of the ligand (entry 4 vs 10). Such rigidity might also be a factor in the low activity of the complex with $\mathbf{L^1PhL^1}$ (entry 13). The presence of pyrazole moieties instead of pyridyl groups stabilizes the Cu^I oxidation state (Chapter 5), which is reflected in the negative effect on the catalytic activity (entry 14-15).

Table 7.5: Turnover frequencies of the oxidation of 3,5-DTBC to 3,5-DTBQ catalyzed by $[Cu^{II}_2(\mathbf{L^{Pz}SSL^{Pz}})]^{4+}$ in the presence of different chloride concentrations.[a]

Catalyst	Graph type[c]	max. TOF (h^{-1})	initial TOF (h^{-1})	Cl^- conc (mM)
$[Cu^{II}_2(\mathbf{L^{Pz}SSL^{Pz}})](BF_4)_4$[b]	C	550	220	0
$[Cu^{II}_2(\mathbf{L^{Pz}SSL^{Pz}})(Cl)_2](BF_4)_2$	C	390	240	0.4
$Cu^{II}_2(\mathbf{L^{Pz}SSL^{Pz}})Cl_4$[b]	C	360	140	0.8
$[Cu^{II}_2(\mathbf{L^{Pz}SSL^{Pz}})(Cl)_2](BF_4)_2$ + Bu_4NCl	C	230	100	20

[a] Reaction conditions: 0.4 mM [Cu], 20 mM 3,5-DTBC, 20 mM NEt_3 in 3 mL CH_3CN. TOFs were determined from the change in absorbance of 3,5-DTBQ at 400 nm.
[b] Complex was formed in situ
[c] The three different types of graphs A, B and C are depicted in Figure 7.8.

The catalytic activity decreases with increasing concentration of chloride ions, as can be seen in Table 7.5. The absorption spectra for $[Cu^{II}_2(\mathbf{L^{Pz}SSL^{Pz}})]^{4+}$ with 1-5 equivalents of chloride ions (in ratio to the dinuclear complex) have been recorded. The spectroscopic changes that are observed upon addition of 1-4 equivalents of chloride ions indicate coordination of the chloride ions to the copper center. During catalysis, the coordinated chloride ions will hamper binding of the substrate or activation of dioxygen. Addition of a fifth equivalent of Cl^- results in formation of an absorption band at 460 nm, which can be attributed to the formation of the complex anion $CuCl_4^{2-}$ (Appendix VI, Figure AVI.5).[23-25] As mentioned before, an abrupt increase is observed in the absorption at 400 nm at the start of the reaction. This 'jump' is likely caused by a change in absorption spectrum when the chloride ions dissociate from the copper center. In other words, the change in absorption at 400 nm can be attributed to a change in the $Cu^{II} \leftarrow Cl$ LMCT. This conclusion is in agreement with the absence of the 'jump' when the 3,5-DTBC oxidation is carried out in either the presence of an excess of chloride ions or the absence of chloride ions (Appendix VI, Figure AVI.6). It is clear that when chloride ions are not present in solution, the change in LMCT will not occur. In the presence of an excess of chloride ions, part of the copper centers dissociate from the ligand to form $CuCl_4^{2-}$ complex anions. Chloride dissociation is suppressed by the excess of chloride ions, resulting in the absence of an abrupt 'jump' in the absorption curve and leading to lower activity.
The catalytic system obtained with $[Cu^{II}_2(\mathbf{L^{1*}SSL^{1*}})(Cl)_2]_n(BF_4)_{2n}$ shows the highest initial TOF with 4700 turnovers h^{-1} (entry 4). As it was found that the presence of chloride ions has a negative effect on the catalytic activity of the catalyst based on the ligand $\mathbf{L^{Pz}SSL^{Pz}}$ (Table 7.5), the catalytic system comprising $\mathbf{L^{1*}SSL^{1*}}$ in the absence of chlorides was also tested. The compound $[Cu^{II}_2(\mathbf{L^{1*}SSL^{1*}})](BF_4)_4$ was formed in situ

by adding two equivalents of $[Cu^{II}(H_2O)_6](BF_4)_2$ to **L¹*SSL¹*** and removing the majority of the H_2O with Na_2SO_4. At 0.4 mM [Cu] concentration the initial TOF of this catalytic system was found to be as high as 7800 h^{-1}. At lower catalyst concentrations the rate of the reaction levels off more quickly (Appendix VI, Figure AVI.7). Since the substrate/catalyst ratio is relatively large at lower catalyst concentrations, this phenomenon is not due to depletion of substrate but can rather be ascribed to more rapid catalyst degradation.

7.3 Discussion

A large library of Cu^{II} complexes has been synthesized and investigated for their catalytic activity in the oxidation of 3,5-DTBC. Crystal structures of a number of the Cu^{II} complexes of dinucleating ligands show that in these cases the chloride ions bridge between the Cu^{II} centers of neighboring molecules, forming polymeric chains. The Cu^{II} complexes with mononucleating ligands form dimeric species in some cases, depending on the coordination geometry of the copper ion. A square-pyramidal geometry of the copper center leaves the sixth coordination site open for coordination to the chloride ion of a molecule in a neighboring subunit.

The oxidation of 3,5-DTBC was carried out with different catalytic systems; three types of reactivity were observed with an increasing, decreasing or constant oxidation rate (Figure 7.8). This variance in catalyst behavior indicates that different activation mechanisms are operative in the formation of the active species depending on the ligand. Catalytic systems that show development of the product following type A have the highest activity at the start of the experiment and become slower over time. For the slower catalytic systems, this type of behavior indicates catalyst degradation over time. However, for the faster catalytic systems like $[Cu^{II}_2(\mathbf{L^{1}*SSL^{1}*})](BF_4)_4$, the decrease in catalytic activity may also be due to depletion of the substrate. The catalysts containing **L¹OH** and **L¹NH₂** show constant activity during the entire experiment (type B), indicating that there is no deactivation of the catalyst. All the other catalysts show an induction period in their activity (type C), which indicates the presence of a pre-catalyst at the beginning of the reaction that is converted to the active catalyst (possibly the Cu^{II} μ-hydroxo species) later on. The ligands **L¹OH** and **L¹NH₂** contain a proton donor/acceptor moiety, which might explain the absence of a similar induction period for these catalysts.

The presence of chloride ions has a negative effect on the catalytic activity. The chloride ions inhibit the reaction either by competing with the substrate for coordination sites or by formation of $CuCl_4^{2-}$, resulting in lower concentration of the

active species in solution. The ease of formation of $CuCl_4^{2-}$ is demonstrated by the structure of the compound $[Cu^{II}(\mathbf{L^1{*}SCH_3})(Cl)]_2(CuCl_4)$, which even formed in the presence of a substoichiometric amount of copper (Appendix VI, Figure AVI.2). Similar behavior was observed for $\mathbf{L^1SXSL^1}$ (Chapter 5).

When comparing the catalytic rates of the different systems (Table 7.4), it is clear that many of the systems under study are not (much) more active than the blank system comprising copper salts in the absence of a ligand. The relative differences however, are very large. The mononuclear catalysts generally have a low TOF, which is not surprising considering that the active species has been proposed to be dinuclear.[7] A number of the systems containing dinucleating ligands behave as mononuclear catalysts, because they are too rigid (entry 10 and 13) or lack bridging sulfur donor atoms (entry 12). Several other dinucleating ligands stabilize the Cu^I oxidation state, also resulting in low activity (entry 7, 9, 14 and 15).[1, 2] The catalytic systems with the highest activity are those containing ligands that stabilize Cu^{II} μ-thiolate complexes ($\mathbf{L^1SSL^1}$, $\mathbf{L^1{*}SSL^1{*}}$, $\mathbf{L^2SSL^2}$, $\mathbf{L^2{*}SSL^2{*}}$, $\mathbf{L^4SSL^4}$).[1, 2, 16, 26] The compound $[Cu^{II}_2(\mathbf{L^2SSL^2})(Cl)_2]_n(BF_4)_{2n}$ forms an exception with its relatively low activity, which can be explained by the fact that $\mathbf{L^2SSL^2}$ forms a Cu^I disulfide complex in CH_3CN which is also the solvent used for catalysis (Chapter 2).[2] These catalytic systems all show catalytic absorption profile A indicating complex degradation, which is not surprising, since Cu^{II} μ-thiolate complexes have been reported either to be oxidized to Cu^{II} sulfinate and sulfonate complexes or to react with the substrate.[10, 27] The rate of 7800 h^{-1} observed for $[Cu^{II}_2(\mathbf{L^1{*}SSL^1{*}})](BF_4)_4$ is the second highest rate reported for 3,5-DTBC oxidation in CH_3CN thus far.[8, 28] It may be argued that this high activity stems from the ability of these complexes to stabilize a Cu^{II}_2 μ-η^2:η^2-peroxide species as it is structurally as well as electronically similar to the Cu^{II} μ-thiolate complex (Figure 7.1), and especially since the formation of this species is proposed to be the rate-determining step of the reaction.[6, 29, 30] Another explanation of the high activity of our catalytic systems might be the participation of the Cu^{II} μ-thiolate complex in catalysis, cycling between Cu^I and Cu^{II} thiolate species. The activity of these catalytic systems can probably be increased even further by using a protic solvent like methanol, but this might also result in faster catalyst degradation.

7.4 Conclusion

Cu^{II} complexes have been synthesized comprising either mononucleating or dinucleating ligands for the catalytic oxidation of 3,5-DTBC. Very high activity for the oxidation of 3,5-DTBC is achieved using ligands that have the ability to form Cu^{II} μ-

thiolate complexes. The presence of chloride ions has a negative effect on the catalytic rates because of coordination to the active sites or the formation of $Cu^{II}Cl_4^{2-}$. The highest TOF reached is 7800 h^{-1} using $[Cu^{II}_2(\mathbf{L^{1*}SSL^{1*}})](BF_4)_4$, which is one of the highest TOFs reported for 3,5-DTBC oxidation in CH_3CN thus far. These results show that there are similarities between thiolato copper and (per)oxido copper chemistry and that ligands that stabilize Cu^{II} μ-thiolate complexes might also induce the formation of Cu^{II}_2 μ-η^2:η^2-peroxide species.

7.5 Experimental section

7.5.1 General methods

Reagents and solvents were purchased from commercial sources. **L^1SSL^1**, **L^2SSL^2**, **L^3SSL^3**, **L^4SSL^4**, **L^5SSL^5**,[1, 2] **$L^{1*}SSL^{1*}$**, **$L^{2*}SSL^{2*}$**,[16] **L^1SXSL^1**, **$L^{Pz}SSL^{Pz}$**, **$L^{MPz}SSL^{MPz}$**, $[Cu^{II}_2(\mathbf{L^{Pz}SSL^{Pz}})(Cl)_2]_n(BF_4)_{2n}$, $[Cu^{II}_2(\mathbf{L^{MPz}SSL^{MPz}})(Cl)_2]_n(BF_4)_{2n}$ (Chapter 5), **$L^1C_6L^1$**,[11] **L^1PhL^1**,[12, 13] **Py_3N**,[14] **L^1SCH_3**, $[Cu^{II}(\mathbf{L^1SCH_3})(Cl)](BF_4)$ (Chapter 6), **L^1NH_2**[22] and 1,5-diamino-3-thiapentane dihydrobromide[17] were synthesized according to literature procedures. NMR spectra were recorded on a Bruker 300 DPX spectrometer. IR spectra were obtained on a Perkin Elmer UATR (Single Reflection Diamond) Spectrum Two device (4000-700 cm^{-1}; resolution 4 cm^{-1}). Mass spectrometry was measured using a Finnigan Aqua Mass Spectrometer (MS) with electro spray ionization (ESI). Sample introduction was achieved through a Dionex ASI-100 automated sample injector with an eluent flow rate of 0.2 mL/min. Elemental analyses were performed using a Perkin Elmer 2400 Series II CHNS/O analyzer or were performed by the Microanalytical laboratory Kolbe in Germany. UV-vis absorbance spectra were recorded on a Varian Cary50 spectrophotometer or using a transmission dipprobe with variable path length on an Avantes Avaspec-2048 spectrometer with Avalight-DH-S-BAL light source.

7.5.2 X-ray Crystallography

$[Cu^{II}_2(\mathbf{L^1SL^1})(Cl)_2]_n(BF_4)_{2n}$ and $[Cu^{II}(\mathbf{L^1NH_2})(Cl)](BF_4)$

The reflection intensities for $[Cu^{II}_2(\mathbf{L^1SL^1})(Cl)_2]_n(BF_4)_{2n}$ and $[Cu^{II}(\mathbf{L^1NH_2})(Cl)](BF_4)$ were measured at 110(2) K using a KM4/Xcalibur (detector: Sapphire3) with enhanced graphite-monochromated Mo *Kα* radiation (λ = 0.71073 Å) under the program CrysAlisPro (Version 1.171.36.24 Agilent Technologies, 2012). The same program was used to refine the cell dimensions and for data reduction. The structures were solved with the program SHELXS-2013 (Sheldrick, 2013)[31] and was refined on F^2 with SHELXL-2013 (Sheldrick, 2013).[31] Analytical numeric absorption corrections based on a multifaceted crystal model were applied using CrysAlisPro. The temperature of the data collection was controlled using the system Cryojet (manufactured by Oxford Instruments). The H atoms were placed at calculated positions using the instructions AFIX 23 or AFIX 43 with isotropic displacement parameters having values 1.2 times *U*eq of the attached C atoms. The H atoms attached to N2 of $[Cu^{II}(\mathbf{L^1NH_2})(Cl)](BF_4)$ were

found from difference Fourier map, and their coordinates and isotropic temperature factors were refined freely.

*[Cu^{II}(**L^{2}SCH$_3$**)(Cl)](BF$_4$) and [Cu^{II}(**L^{3}SCH$_3$**)(Cl)](BF$_4$)*

The reflection intensities for [Cu^{II}(**L^{2}SCH$_3$**)(Cl)](BF$_4$) and [Cu^{II}(**L^{3}SCH$_3$**)(Cl)](BF$_4$) were measured at 110(2) K using a SuperNova diffractometer (equipped with Atlas detector) with Cu *Kα* radiation (λ = 1.54178 Å) under the program CrysAlisPro (Version 1.171.36.32 Agilent Technologies, 2013). The same program was used to refine the cell dimensions and for data reduction. The structures were solved with the program SHELXS-2013 (Sheldrick, 2013)[31] and were refined on F^2 with SHELXL-2013 (Sheldrick, 2013).[31] Analytical numeric absorption corrections based on a multifaceted crystal model were applied using CrysAlisPro. The temperature of the data collection was controlled using the system Cryojet (manufactured by Oxford Instruments). The H atoms were placed at calculated positions using the instructions AFIX 23, AFIX 43 or AFIX 137 with isotropic displacement parameters having values 1.2 or 1.5 times *U*eq of the attached C atoms.

*[Cu$^{II}_2$(**L^{1}C$_6$L^1**)(Cl)$_2$]$_n$(BF$_4$)$_{2n}$*

The reflection intensities for [Cu$^{II}_2$(**L^{1}C$_6$L^1**)(Cl)$_2$]$_n$(BF$_4$)$_{2n}$ were measured on a Bruker Kappa Apex II diffractometer with sealed tube and Triumph monochromator (λ = 0.71073 Å) up to a resolution of $(\sin\theta/\lambda)_{max}$ = 0.57 Å^{-1}. The crystal consisted of several fragments. The four major fragments were taken into account during the integration with the Eval14 software.[32] The second fragment has an arbitrary orientation with respect to the first. The third fragment is generated by a twofold rotation about hkl=(1,0,0) from the first. The fourth fragment has the same twin relation to the second. An absorption correction based on multiple measured reflections was performed with TWINABS (0.57-0.75 correction range).[33] The structure was solved with Direct Methods using SHELXS-97 and refined with SHELXL-97 against F^2 of all reflections.[31] The presence of four fragments was handled with a HKLF-5 reflection file.[34] The twin fractions refined to 0.342(15), 0.267(7), and 0.083(4). Non-hydrogen atoms were refined freely with anisotropic displacement parameters. Hydrogen atoms were introduced in calculated positions and refined with a riding model. The BF_4^- anion was refined with a disorder model of two orientations. Geometry calculations and checking for higher symmetry was performed with the PLATON program.[35]

7.5.3 Ligand synthesis

*Bis-1,5-((2-pyridylmethyl)amino)ethyl-3-thiapentane (**L^{1}SL^1**)*

1,5-Diamino-3-thiapentane dihydrobromide (1.43 g, 5.1 mmol) was dissolved in methanol (40 mL). To this solution 2-pyridinecarboxaldehyde (1.9 mL, 20.3 mmol) was added, after which the reaction mixture was cooled to 0 °C. $NaBH_3CN$ (1.28 g, 20.3 mmol) was added in small portions. The reaction mixture was allowed to warm up to RT and was stirred for 3 days. The reaction mixture was quenched by addition of HCl (37%) until pH = 1. After evaporation of the

solvent, the product was treated with NaOH (50 mL; 5 M) and the aqueous layer was extracted with $CHCl_3$ (3 x 25 mL). The organic fractions were combined, dried over $MgSO_4$ and evaporated to dryness yielding **L^1SL^1** as a brown oil (1.68 g, 3.5 mmol, 68%). ^{1}H NMR (300 MHz, CD_3OD, RT): δ 2.64 (m, 8H, S-CH_2-CH_2), 3.76 (s, 8H, Py-CH_2-N), 7.21 (m, 4H, Py-H_5), 7.62 (d, J = 8 Hz, 4H, Py-H_3), 7.72 (dt, J = 8 Hz, 2 Hz, 4H, Py-H_4), 8.41 (m, 4H, Py-H_6). ^{13}C NMR (75 MHz, CD_3OD, RT): δ 30.5 (S-CH_2-CH_2), 55.1 (S-CH_2-CH_2), 60.7 (Py-CH_2-N), 123.6 (Py-C_5), 124.6 (Py-C_3), 138.4 (Py-C_4), 149.3 (Py-C_6), 160.4 (Py-C_2). ESI-MS found (calculated) for $[M + H]^+$ m/z 485.1 (485.3); $[M + Na]^+$ m/z 507.1 (507.2). IR (neat, cm^{-1}): 3050*w*, 2924*w*, 2821*m*, 1589*s*, 1569*m*, 1473*m*, 1432*s*, 1362*m*, 1265*w*, 1147*m*, 1117*m*, 1086*m*, 1047*m*, 994*m*, 978*m*, 895*w*, 755*vs*, 731*vs*, 701*m*, 613*m*, 465*w*.

*L^1*SCH$_3$*

A mixture of bis(2-pyridylmethyl)amine (1.44 mL, 8.0 mmol) and propylene sulfide (0.94 mL, 12.0 mmol) was stirred in 20 mL CH_3CN at reflux temperature for 18 hrs under Ar atmosphere. The solvent was evaporated, after which the resulting oil was dissolved in 20 mL tetrahydrofuran. NaH (0.37 g, 9.3 mmol, 60% in mineral oil) was added and the reaction mixture was stirred for 2 hrs. To this pink reaction mixture, MeI (0.51 mL, 8.2 mmol) was added and all was stirred for 5 hrs. The reaction was quenched by dropwise addition of H_2O. In total 40 mL H_2O was added after which the water layer was extracted with CH_2Cl_2 (3 × 30 mL). The combined organic layers were dried over Na_2SO_4. The crude product was purified by column chromatography over basic alumina (50/50 EtOAc/petroleum ether) to yield **L^1*SCH$_3$** as a light yellow oil (1.98 g, 6.9 mmol, 86%). ^{1}H NMR (300 MHz, CD_3OD, RT): δ 1.18 (s, 1.5H, C*-CH_3), 1.20 (s, 1.5H, C*-CH_3), 1.99 (s, 3H, S-CH_3), 2.52 (dd, J = 13 Hz, 8 Hz, 1H, N-CH_2-C*), 2.68 (dd, J = 13 Hz, 7 Hz, 1H, N-CH_2-C*), 2.86 (dt, J = 8 Hz, 7 Hz, 1H, C*-H), 3.81 (s, 4H, Py-CH_2-N), 7.30 (ddd, J = 7 Hz, 5 Hz, 1 Hz, 2H, Py-H_5), 7.71 (d, J = 8 Hz, 2H, Py-H_3), 7.82 (td, J = 8 Hz, 2 Hz, 2H, Py-H_4), 8.43 (ddd, J = 5 Hz, 2 Hz, 1 Hz, 2H, Py-H_6). ^{13}C NMR (75 MHz, CD_3OD, RT): δ 13.0 (S-CH_3), 19.5 (C*-CH_3), 40.3 (C*), 61.4 (N-CH_2-C*), 61.5 (Py-CH_2-N), 123.8 (Py-C_5), 125.1 (Py-C_3), 138.5 (Py-C_4), 149.3 (Py-C_6), 160.5 (Py-C_2). ESI-MS found (calculated) for $[M + H]^+$ m/z 288.1 (288.2). IR (neat, cm^{-1}): 3392*br*, 2961*w*, 2919*m*, 2822*w*, 1663*w*, 1589*s*, 1569*m*, 1473*m*, 1432*s*, 1365*m*, 1300*w*, 1247*w*, 1148*m*, 1125*w*, 1075*m*, 1047*m*, 995*m*, 981*m*, 957*m*, 759*vs*, 613*m*, 525*m*, 460*m*.

N-((6-methylpyridin-2-yl)methyl)-2-(methylthio)ethylamine

2-(Methylthio)ethylamine (1.00 g, 11.0 mmol) and 6-methylpyridine-2-carboxaldehyde (1.34 g, 11.0 mmol) were dissolved in 35 mL methanol and stirred at reflux temperature for 24 hrs. The dark orange solution was cooled to RT, after which $NaBH_4$ (0.64 g, 16.9 mmol) was added and the reaction mixture was stirred for 3 hrs. The solvent was evaporated and 30 mL H_2O and 30 mL CH_2Cl_2 were added. The layers were separated and the aqueous layer was extracted CH_2Cl_2 (2 × 30 mL). The combined organic layers were dried over Na_2SO_4 and the solvent was evaporated to yield *N*-((6-methylpyridin-2-yl)methyl)-2-(methylthio)ethylamine in quantitative yield as a red/brown oil. ^{1}H NMR (300 MHz, CD_3OD, RT): δ 2.04 (s, 3H, S-CH_3), 2.52 (s, 3H, Py-

CH_3), 2.65 (m, 2H, S-CH_2-CH_2), 2.79 (m, 2H, S-CH_2-CH_2), 3.85 (s, 2H, Py-CH_2-N), 7.14 (d, J = 8 Hz, 1H, Py-H_3), 7.23 (d, J = 8 Hz, 1H, Py-H_5), 7.66 (t, J = 8 Hz, 1H, Py-H_4). ^{13}C NMR (75 MHz, CD_3OD, RT): δ 15.1 (S-CH_3), 24.1 (Py-CH_3), 34.5 (S-CH_2-CH_2), 48.1 (S-CH_2-CH_2), 54.8 (Py-CH_2-N), 120.9 (Py-C_5), 123.1 (Py-C_3), 138.7 (Py-C_4), 159.0 (Py-C_6), 159.5 (Py-C_2).

L²SCH₃

N-((6-methylpyridin-2-yl)methyl)-2-(methylthio)ethylamine (1.28 g, 6.5 mmol) and 2-pyridinecarboxaldehyde (0.62 mL, 6.5 mmol) were dissolved in 20 mL methanol and stirred at reflux temperature for 2 hrs. The dark brown solution was cooled to RT, $NaBH_4$ (0.39 g, 10.4 mmol) was added and the reaction mixture was stirred for 3 hrs. The solvent was evaporated and 20 mL H_2O and 20 mL CH_2Cl_2 was added. The layers were separated and the aqueous layer was extracted with CH_2Cl_2 (2 × 20 mL). The combined organic layers were dried over Na_2SO_4 and the solvent was evaporated to yield a brown oil (1.84 g). The compound was purified by column chromatography over basic alumina (30/70 EtOAc/petroleum ether) to yield **L²SCH₃** as a yellow/orange oil (0.93 g, 3.2 mmol, 50%). ^{1}H NMR (300 MHz, CD_3OD, RT): δ 1.59 (s, 3H, S-CH_3), 2.47 (s, 3H, Py$_{Me}$-CH_3), 2.64 (m, 2H, S-CH_2-CH_2), 2.75 (m, 2H, S-CH_2-CH_2), 3.79 (s, 2H, Py-CH_2-N), 3.82 (s, 2H, Py-CH_2-N), 7.09 (d, J = 8 Hz, 1H, Py$_{Me}$-H_3), 7.24 (ddd, J = 7 Hz, 5 Hz, 1 Hz, 1H, Py$_{Me}$-H_5), 7.47 (d, J = 8 Hz, 1H, Py-H_3), 7.65 (m, 2H, Py-H_4; Py$_{Me}$-H_4), 7.77 (td, J = 8 Hz, 2 Hz, 1H, Py-H_5), 8.42 (d, J = 5 Hz, 1H, Py-H_6). ^{13}C NMR (75 MHz, CD_3OD, RT): δ 15.6 (S-CH_3), 23.9 (Py-CH_3), 32.5 (S-CH_2-CH_2), 54.7 (S-CH_2-CH_2), 60.8 (Py-CH_2-N), 60.8 (Py-CH_2-N), 121.6 (Py$_{Me}$-C_5), 123.1 (Py$_{Me}$-C_3), 123.7 (Py-C_5), 124.8 (Py-C_3), 138.5 (Py$_{Me}$-C_4), 138.7 (Py-C_4), 149.3 (Py-C_6), 158.5 (Py$_{Me}$-C_2), 159.9 (Py$_{Me}$-C_6), 160.6 (Py-C_2). ESI-MS found (calculated) for $[M + H]^+$ m/z 288.1 (288.2). IR (neat, cm^{-1}): 3393*w*, 3061*w*, 2916*m*, 2828*m*, 1591*s*, 1577*s*, 1456*s*, 1433*s*, 1363*m*, 1290*w*, 1152*m*, 1118*m*, 1089*m*, 1047*m*, 994*m*, 783*s*, 756*vs*, 614*m*, 545*m*.

L³SCH₃

N-((6-methylpyridin-2-yl)methyl)-2-(methylthio)ethylamine (1.28 g, 6.5 mmol) and 6-methylpyridine-2-carboxaldehyde (0.79 g, 6.5 mmol) were dissolved in 20 mL methanol and stirred at reflux temperature for 18 hrs. The brown solution was cooled to RT and $NaBH_4$ (0.37 g, 9.8 mmol) was added and the reaction mixture was stirred for 2 hrs. The solvent was evaporated and 20 mL H_2O and 20 mL CH_2Cl_2 were added. The layers were separated and the aqueous layer was extracted two more times with 20 mL CH_2Cl_2. The combined organic layers were dried over Na_2SO_4 and the solvent was evaporated to yield a brown oil (1.93 g). The compound was purified by column chromatography over basic alumina (30/70 EtOAc/petroleum ether) to yield **L³SCH₃** as a yellow/orange oil (0.91 g, 3.0 mmol, 46%). ^{1}H NMR (300 MHz, CD_3OD, RT): δ 1.95 (s, 3H, S-CH_3), 2.47 (s, 6H, Py-CH_3), 2.64 (m, 2H, S-CH_2-CH_2), 2.74 (m, 2H, S-CH_2-CH_2), 3.78 (s, 4H, Py-CH_2-N), 7.08 (d, J = 8 Hz, 2H, Py-H_3), 7.47 (d, J = 8 Hz, 2H, Py-H_5), 7.63 (t, J = 8 Hz, 2H, Py-H_4). ^{13}C NMR (75 MHz, CD_3OD, RT): δ 15.6 (S-CH_3), 23.9 (Py-CH_3), 32.6 (S-CH_2-CH_2), 54.7 (S-CH_2-CH_2), 60.8 (Py-CH_2-N), 121.5 (Py-C_5), 123.1 (Py-C_3), 138.7 (Py-C_4), 158.5 (Py-C_6), 160.1 (Py-C_2). ESI-MS found (calculated) for $[M + H]^+$ m/z 302.1

(302.2). IR (neat, cm^{-1}): 3388*w*, 3061*w*, 2917*m*, 2829*w*, 1592*s*, 1577*s*, 1456*s*, 1375*m*, 1355*m*, 1291*w*, 1154*m*, 1117*m*, 1090*m*, 1035*m*, 994*m*, 972*m*, 786*s*, 760*m*, 627*m*, 546*m*.

L^1OH

This ligand was synthesized using a modified literature procedure.[14, 19] 2-Pyridinecarboxaldehyde (1.90 mL, 20.0 mmol) was added to ethanolamine (0.60 mL, 10.0 mmol) dissolved in 30 mL CH_2Cl_2. $NaBH(OAc)_3$ (6.0 g, 28.3 mmol) was added in portions over 15 min. after which the reaction mixture was stirred for 4 hrs. The reaction was quenched by addition of 40 mL $NaHCO_3$ (sat.). The layers were separated and the aqueous layer was extracted two more times with 20 mL CH_2Cl_2. The combined organic layers were dried over Na_2SO_4 and then evaporated to dryness yielding **L^1OH** as a yellow oil. (2.41 g, 9.9 mmol, 99%). ^1H NMR (300 MHz, CD_3CN, RT): δ 2.71 (t, *J* = 6 Hz, 2H, S-CH_2-CH_2), 3.56 (t, *J* = 6 Hz, 2H, S-CH_2-CH_2), 3.83 (s, 4H, Py-CH_2-N), 4.0 (br, CH_2-O*H*), 7.17 (m, 2H, Py-*H*5), 7.43 (d, *J* = 8 Hz, 2H, Py-*H*3), 7.66 (td, *J* = 8 Hz, 2 Hz, 2H, Py-*H*4), 8.47 (d, *J* = 5 Hz, 2H, Py-*H*6). ^{13}C NMR (75 MHz, CD_3CN, RT): δ 57.5 (S-*C*H_2-*C*H_2), 60.3 (S-*C*H_2-*C*H_2), 61.0 (Py-*C*H_2-N), 123.0 (Py-*C*3/Py-*C*5), 123.9 (Py-*C*3/Py-*C*5), 137.4 (Py-*C*4), 149.8 (Py-*C*6), 160.8 (Py-*C*2). ESI-MS found (calculated) for $[M + H]^+$ *m*/*z* 244.2 (244.1). IR (neat, cm^{-1}): 3270*br*, 2939*w*, 2826*m*, 1592*s*, 1570*m*, 1475*m*, 1433*s*, 1363*m*, 1309*w*, 1249*w*, 1149*m*, 1047*s*, 1002*m*, 758*vs*, 616*s*, 502*m*, 469*m*.

Py_2S

This ligand was synthesized using a modified literature procedure.[18] NaOH (0.30 g, 7.5 mmol) was dissolved in a mixture of 10 mL H_2O and 10 mL ethanol. $Na_2S \cdot 9\ H_2O$ (0.60 g, 2.5 mmol) and 2-(chloromethyl)pyridine hydrochloride (0.82 g, 5.0 mmol) were added. The mixture was refluxed at 95°C for 20 hours and left to cool to RT. The resulting bright orange solution was extracted twice with 20 mL CH_2Cl_2. The organic fractions were combined and dried over Na_2SO_4 to yield **Py_2S** as a yellow oil (0.48 g, 2.2 mmol, 88%). ^1H NMR (300 MHz, CD_3OD, RT): δ 3.82 (s, 4H, S-CH_2-N), 7.25 (dd, *J* = 7 Hz, 5 Hz, 2H, Py-*H*5), 7.42 (d, *J* = 8 Hz, 2H, Py-*H*3), 7.73 (td, *J* = 8 Hz, 2 Hz, 2H, Py-*H*4), 8.42 (d, *J* = 5 Hz, 2H, Py-*H*6). ^{13}C NMR (75 MHz, CD_3OD, RT): δ 38.2 (S-*C*H_2-N), 123.5 (Py-*C*5), 124.9 (Py-*C*3), 138.7 (Py-*C*4), 149.7 (Py-*C*6), 159.4 (Py-*C*2). ESI-MS found (calculated) for $[M + H]^+$ *m*/*z* 217.1 (217.1). IR (neat, cm^{-1}): 3369*br*, 3050*w*, 3008*w*, 2925*w*, 1590*s*, 1568*m*, 1471*m*, 1434*vs*, 1307*w*, 1208*w*, 1151*w*, 1088*w*, 1048*w*, 994*m*, 790*m*, 747*vs*, 711*m*, 627*w*, 579*m*, 484*m*.

7.5.4 Complex synthesis

General synthesis procedure

All complexes were synthesized in the same manner unless mentioned otherwise. The ligand was dissolved in methanol, after which $[Cu^{II}(H_2O)_6](BF_4)_2$ and $Cu^{II}Cl_2 \cdot 2\ H_2O$ were added. If there was no formation of powder, diethyl ether was added until precipitation occured. The powder was filtered and washed with diethyl ether to yield the target complex.

*[Cu^{II}_2(**L^1SSL^1**)$(Cl)_2]_n(BF_4)_{2n}$*

From **L^1SSL^1** (67 mg; 0.13 mmol), $[Cu^{II}(H_2O)_6](BF_4)_2$ (46 mg; 0.13 mmol) and $Cu^{II}Cl_2 \cdot 2\ H_2O$ (22 mg; 0.13 mmol), the product $[Cu^{II}_2$(**L^1SSL^1**$)(Cl)_2]_n(BF_4)_{2n}$ (104 mg; 0.12 mmol; 90%) was obtained as a blue powder. Crystals suitable for X-ray structure determination were obtained by slow vapor diffusion of diethyl ether into a CH_3CN solution containing the complex. ESI-MS found (calculated) for $[M - 2\ BF_4]^+$ *m/z* 357.0 (357.0); $[½\ M - Cl - BF_4]^+$ *m/z* 320.9 (321.0); $[½\ M + Cl - BF_4]^+$ *m/z* 392.9 (393.0). IR (neat, cm^{-1}): 1610*m*, 1575*w*, 1486*w*, 1447*m*, 1303*w*, 1286*w*, 1026*vs*, 990*s*, 921*m*, 820*w*, 777*m*, 762*s*, 719*m*, 656*w*, 518*m*, 476*w*, 424*s*. Elemental analysis calcd for $[Cu^{II}_2$(**L^1SSL^1**$)(Cl)_2](BF_4)_2 \cdot H_2O$: C 37.11, H 3.78, N 9.27, S 7.07; Found: C 37.40, H 3.96, N 9.25, S 7.23. UV-vis in CH_3CN at 0.1 mM [Cu] concentration: 258 nm (ε = 10 300 $M^{-1}\ cm^{-1}$), 289 nm (ε = 2 700 $M^{-1}\ cm^{-1}$), 680 nm (ε = 190 $M^{-1}\ cm^{-1}$).

*[Cu^{II}_2(**L^1*SSL^1***$)(Cl)_2]_n(BF_4)_{2n}$*

From **L^1*SSL^1*** (197 mg; 0.36 mmol), $[Cu^{II}(H_2O)_6](BF_4)_2$ (128 mg; 0.36 mmol) and $Cu^{II}Cl_2 \cdot 2\ H_2O$ (62 mg; 0.36 mmol), the product $[Cu^{II}_2$(**L^1*SSL^1***$)(Cl)_2]_n(BF_4)_{2n}$ (245 mg; 0.27 mmol; 74%) was obtained as a blue powder. ESI-MS found (calculated) for $[M - 2\ BF_4]^{2+}$ *m/z* 371.0 (371.0); $[M + 2\ Cl - 2\ BF_4]^{2+}$ *m/z* 407.0 (406.0); $[½\ M - Cl - BF_4]^+$ *m/z* 335.0 (335.1); $[M - Cu - Cl - 2\ BF_4]^+$ *m/z* 642.3 (642.1). IR (neat, cm^{-1}): 1611*w*, 1574*w*, 1484*w*, 1446*m*, 1284*w*, 1162*w*, 1048*vs*, 1030*vs*, 935*m*, 866*m*, 819*w*, 765*s*, 726*w*, 658*w*, 521*m*, 420*m*. Elemental analysis calcd for $[Cu^{II}_2$(**L^1*SSL^1***$)(Cl)_2](BF_4)_2$: C 39.32, H 3.96, N 9.17, S 7.00; Found: C 38.69, H 3.99, N 9.19, S 6.88. UV-vis in CH_3CN at 0.1 mM [Cu] concentration: 258 nm (ε = 10 900 $M^{-1}\ cm^{-1}$), 294 nm (ε = 2 900 $M^{-1}\ cm^{-1}$), 690 nm (ε = 210 $M^{-1}\ cm^{-1}$).

*[Cu^{II}_2(**L^2SSL^2**)$(Cl)_2]_n(BF_4)_{2n}$*

L^2SSL^2 (72 mg; 0.13 mmol), $[Cu^{II}(H_2O)_6](BF_4)_2$ (46 mg; 0.13 mmol) and $Cu^{II}Cl_2 \cdot 2\ H_2O$ (23 mg; 0.13 mmol) were dissolved in 5 mL CH_3CN. Diethyl ether (13 mL) was added to the bright blue solution. After 15 minutes, the suspension was decanted and filtered. This yielded a bright blue powder that was washed with diethyl ether giving $[Cu^{II}_2$(**L^2SSL^2**$)(Cl)_2]_n(BF_4)_{2n}$ (48 mg; 0.05 mmol; 40%). Single crystals suitable for X-ray structure determination were synthesized from $[Cu^{II}(H_2O)_6](ClO_4)_2$ instead of $[Cu^{II}(H_2O)_6](BF_4)_2$. Slow vapor diffusion of diethyl ether into a CH_3CN solution containing the complex, yielded crystals of $[Cu^{II}_2$(**L^2SSL^2**$)(Cl)_2]_n(ClO_4)_{2n}$. ESI-MS found (calculated) for $[M - 2\ BF_4]^{2+}$ *m/z* 371.0 (371.0); $[M + 2\ Cl - 2\ BF_4]^{2+}$ *m/z* 406.9 (406.0); $[½\ M - Cl - BF_4]^+$ *m/z* 335.0 (335.1). IR (neat, cm^{-1}): 3554*w*, 1610*m*, 1577*w*, 1447*m*, 1287*w*, 1052*vs*, 1028*vs*, 921*m*, 790*m*, 764*m*, 724*w*, 654*w*, 520*m*, 474*m*. Elemental analysis calcd for $[Cu^{II}_2$(**L^2SSL^2**$)(Cl)_2](BF_4)_2$: C 39.32, H 3.96, N 9.17, S 7.00; Found: C 39.23, H 4.01, N 9.12, S 6.96. UV-vis in CH_3CN at 0.1 mM [Cu] concentration: 263 nm (ε = 11 600 $M^{-1}\ cm^{-1}$), 303 nm (ε = 2 800 $M^{-1}\ cm^{-1}$), 720 nm (ε = 270 $M^{-1}\ cm^{-1}$).

*[Cu^{II}_2(**$L^{2*}SSL^{2*}$**)(Cl)$_2$]$_n$(BF_4)$_{2n}$*

From **$L^{2*}SSL^{2*}$** (84 mg; 0.15 mmol), [Cu^{II}(H_2O)$_6$](BF_4)$_2$ (51 mg; 0.15 mmol) and $Cu^{II}Cl_2 \cdot 2\ H_2O$ (25 mg; 0.15 mmol), the product [Cu^{II}_2(**$L^{2*}SSL^{2*}$**)(Cl)$_2$]$_n$(BF_4)$_{2n}$ (97 mg; 0.10 mmol; 70%) was obtained as a blue powder. ESI-MS found (calculated) for [M – 2 BF_4]$^{2+}$ *m/z* 386.0 (385.0); [½ M – Cl – BF_4]$^+$ *m/z* 349.1 (349.1); [½ M + Cl – BF_4]$^+$ *m/z* 421.0 (421.0); [M – Cu – Cl – 2 BF_4]$^+$ *m/z* 670.3 (670.2). IR (neat, cm^{-1}): 3565*w*, 2934*w*, 1611*m*, 1576*w*, 1447*m*, 1287*w*, 1052*vs*, 1027*vs*, 867*w*, 771*m*, 729*w*, 654*w*, 521*m*. Elemental analysis calcd for [Cu^{II}_2(**$L^{2*}SSL^{2*}$**)(Cl)$_2$](BF_4)$_2$: C 40.70, H 4.27, N 8.90, S 6.79; Found: C 39.35, H 4.13, N 8.52, S 6.85. UV-vis in CH_3CN at 0.1 mM [Cu] concentration: 264 nm (ε = 11 400 M^{-1} cm^{-1}), 303 nm (ε = 3 000 M^{-1} cm^{-1}), 730 nm (ε = 270 M^{-1} cm^{-1}).

*[Cu^{II}_2(**L^3SSL^3**)(Cl)$_2$]$_n$(BF_4)$_{2n}$*

From **L^3SSL^3** (153 mg; 0.27 mmol), [Cu^{II}(H_2O)$_6$](BF_4)$_2$ (93 mg; 0.27 mmol) and $Cu^{II}Cl_2 \cdot 2\ H_2O$ (46 mg; 0.27 mmol), the product [Cu^{II}_2(**L^3SSL^3**)(Cl)$_2$]$_n$(BF_4)$_{2n}$ (207 mg; 0.22 mmol; 82%) was obtained as a blue powder. ESI-MS found (calculated) for [½ M – Cl – BF_4]$^+$ *m/z* 349.0 (349.1); [M – Cu – 2 Cl – 2 BF_4]$^{2+}$ *m/z* 318.1 (317.6); [M – Cu – 2 Cl – 2 BF_4]$^+$ *m/z* 635.3 (635.2). IR (neat, cm^{-1}): 2938*w*, 1612*m*, 1577*w*, 1474*m*, 1459*m*, 1417*w*, 1386*w*, 1349*w*, 1274*w*, 1243*w*, 1172*w*, 1049*vs*, 986*vs*, 923*m*, 852*m*, 805*m*, 722*m*, 519*m*. Elemental analysis calcd for [Cu^{II}_2(**L^3SSL^3**)(Cl)$_2$](BF_4)$_2$: C 40.70, H 4.27, N 8.90, S 6.79; Found: C 39.90, H 4.21, N 8.86, S 6.81. UV-vis in CH_3CN at 0.1 mM [Cu] concentration: 265 nm (ε = 13 000 M^{-1} cm^{-1}), 343 nm (ε = 1 600 M^{-1} cm^{-1}), 640 nm (ε = 180 M^{-1} cm^{-1}), 750 nm (ε = 200 M^{-1} cm^{-1}).

*[Cu^{II}_2(**L^4SSL^4**)(Cl)$_2$]$_n$(BF_4)$_{2n}$*

From **L^4SSL^4** (96 mg; 0.18 mmol), [Cu^{II}(H_2O)$_6$](BF_4)$_2$ (61 mg; 0.18 mmol) and $Cu^{II}Cl_2 \cdot 2\ H_2O$ (30 mg; 0.18 mmol), the product [Cu^{II}_2(**L^4SSL^4**)(Cl)$_2$]$_n$(BF_4)$_{2n}$ (110 mg; 0.12 mmol; 68%) was obtained as a greyish blue powder. ESI-MS found (calculated) for [M – 2 BF_4]$^{2+}$ *m/z* 371.0 (371.0); [M + 2 Cl – 2 BF_4]$^{2+}$ *m/z* 406.9 (406.0); [½ M – Cl – BF_4]$^+$ *m/z* 335.0 (335.1); [M – Cu – Cl – 2 BF_4]$^+$ *m/z* 642.3 (642.1). IR (neat, cm^{-1}): 3628*w*, 1612*m*, 1574*w*, 1487*w*, 1448*m*, 1319*w*, 1300*w*, 1165*w*, 1054*vs*, 1029*vs*, 946*m*, 769*s*, 724*w*, 655*w*, 588*w*, 520*m*, 479*m*. Elemental analysis calcd for [Cu^{II}_2(**L^4SSL^4**)(Cl)$_2$](BF_4)$_2 \cdot H_2O$: C 38.56, H 4.10, N 8.99, S 6.86; Found: C 38.45, H 4.36, N 9.12, S 7.03. UV-vis in CH_3CN at 0.1 mM [Cu] concentration: 261 nm (ε = 11 500 M^{-1} cm^{-1}), 293 nm (ε = 3 600 M^{-1} cm^{-1}), 580 nm (ε = 200 M^{-1} cm^{-1}), 670 nm (ε = 180 M^{-1} cm^{-1}).

*[Cu^{II}_2(**L^5SSL^5**)(Cl)$_2$]$_n$(BF_4)$_{2n}$*

This complex was formed in situ. CH_3CN at 0.1 mM [Cu] concentration: 263 nm (ε = 10 800 M^{-1} cm^{-1}), 292 nm (ε = 3 600 M^{-1} cm^{-1}), 342 nm (ε = 1 900 M^{-1} cm^{-1}), 710 nm (ε = 170 M^{-1} cm^{-1}).

*[Cu^{II}_2(**L^1SXSL^1**)(Cl)$_2$]$_n$(BF_4)$_{2n}$*

From **L^1SXSL^1** (23 mg; 0.04 mmol), [Cu^{II}(H_2O)$_6$](BF_4)$_2$ (15 mg; 0.04 mmol) and $Cu^{II}Cl_2 \cdot 2\ H_2O$ (7.4 mg; 0.04 mmol) in CH_3CN, the product [Cu^{II}_2(**L^1SXSL^1**)(Cl)$_2$]$_n$(BF_4)$_{2n}$ (34 mg; 0.04 mmol;

86%) was obtained as a light blue powder. ESI-MS found (calculated) for $[M - 2\ BF_4]^{2+}$ *m/z* 370.0 (370.0). IR (neat, cm^{-1}): 3612*w*, 1611*m*, 1574*w*, 1484*w*, 1447*m*, 1287*w*, 1162*w*, 1054*vs*, 1030*vs*, 901*w*, 852*w*, 819*w*, 765*s*, 728*w*, 656*w*, 521*m*. Elemental analysis calcd for $[Cu^{II}_2(\mathbf{L^1SXSL^1})(Cl)_2](BF_4)_2$: C 39.41, H 3.75, N 9.19, S 7.01; Found: C 38.56, H 3.73, N 9.04, S 6.85. UV-vis in CH_3CN at 0.1 mM [Cu] concentration: 257 nm (ε = 10 800 $M^{-1}\ cm^{-1}$), 290 nm (ε = 3 000 $M^{-1}\ cm^{-1}$), 700 nm (ε = 190 $M^{-1}\ cm^{-1}$).

$[Cu^{II}_2(\mathbf{L^1SL^1})(Cl)_2]_n(BF_4)_{2n}$

From $\mathbf{L^1SL^1}$ (275 mg; 0.57 mmol), $[Cu^{II}(H_2O)_6](BF_4)_2$ (196 mg; 0.57 mmol) and $Cu^{II}Cl_2 \cdot 2\ H_2O$ (97 mg; 0.57 mmol), the product $[Cu^{II}_2(\mathbf{L^1SL^1})(Cl)_2]_n(BF_4)_{2n}$ (370 mg; 0.43 mmol; 76%) was obtained as a light blue powder. Crystals suitable for X-ray structure determination were obtained by slow vapor diffusion of diethyl ether into a CH_3CN solution containing the complex. ESI-MS found (calculated) for $[M - 2\ BF_4]^{2+}$ *m/z* 341.0 (341.0). IR (neat, cm^{-1}): 3612*w*, 1611*m*, 1574*w*, 1481*w*, 1444*m*, 1290*w*, 1088*m*, 1049*vs*, 1030*vs*, 995*m*, 973*w*, 946*w*, 906*w*, 819*w*, 777*m*, 761*m*, 717*m*, 654*w*, 521*w*. Elemental analysis calcd for $[Cu^{II}_2(\mathbf{L^1SL^1})(Cl)_2](BF_4)_2$: C 39.28, H 3.77, N 9.81, S 3.74; Found: C 40.13, H 3.85, N 10.15, S 3.67. UV-vis in CH_3CN at 0.1 mM [Cu] concentration: 256 nm (ε = 10 600 $M^{-1}\ cm^{-1}$), 290 nm (ε = 2 900 $M^{-1}\ cm^{-1}$), 690 nm (ε = 110 $M^{-1}\ cm^{-1}$).

$[Cu^{II}_2(\mathbf{L^1C_6L^1})(Cl)_2]_n(BF_4)_{2n}$

From $\mathbf{L^1C_6L^1}$ (102 mg; 0.21 mmol), $[Cu^{II}(H_2O)_6](BF_4)_2$ (74 mg; 0.21 mmol) and $Cu^{II}Cl_2 \cdot 2\ H_2O$ (36 mg; 0.21 mmol), the product $[Cu^{II}_2(\mathbf{L^1C_6L^1})(Cl)_2]_n(BF_4)_{2n}$ (158 mg; 0.19 mmol; 87%) was obtained as a dark blue powder. Crystals suitable for X-ray structure determination were obtained by slow vapor diffusion of di-isopropyl ether into a CH_3CN solution containing the complex. ESI-MS found (calculated) for $[M - 2\ BF_4]^{2+}$ *m/z* 339.1 (339.1). IR (neat, cm^{-1}): 3090*w*, 2933*w*, 2853*w*, 1612*m*, 1574*w*, 1484*w*, 1446*m*, 1283*m*, 1088*m*, 1049*vs*, 1031*vs*, 897*m*, 883*m*, 817*w*, 766*s*, 726*w*, 660*w*, 521*m*, 492*w*. Elemental analysis calcd for $[Cu^{II}_2(\mathbf{L^1C_6L^1})(Cl)_2](BF_4)_2$: C 42.28, H 4.26, N 9.86; Found: C 42.49, H 4.35, N 9.93. UV-vis in CH_3CN at 0.1 mM [Cu] concentration: 256 nm (ε = 11 800 $M^{-1}\ cm^{-1}$), 291 nm (ε = 3 000 $M^{-1}\ cm^{-1}$), 660 nm (ε = 140 $M^{-1}\ cm^{-1}$).

$[Cu^{II}_2(\mathbf{L^1PhL^1})(Cl)_2]_n(BF_4)_{2n}$

From $\mathbf{L^1PhL^1}$ (166 mg; 0.35 mmol), $[Cu^{II}(H_2O)_6](BF_4)_2$ (121 mg; 0.35 mmol) and $Cu^{II}Cl_2 \cdot 2\ H_2O$ (60 mg; 0.35 mmol), the product $[Cu^{II}_2(\mathbf{L^1PhL^1})(Cl)_2]_n(BF_4)_{2n}$ (249 mg; 0.30 mmol; 84%) was obtained as a green powder. ESI-MS found (calculated) for $[M - 2\ BF_4]^{2+}$ *m/z* 335.0 (335.0); $[M - Cu - Cl - 2\ BF_4]^{+}$ *m/z* 570.2 (570.1). IR (neat, cm^{-1}): 2972*w*, 1611*m*, 1575*w*, 1486*w*, 1449*m*, 1288*m*, 1052*vs*, 1031*vs*, 870*m*, 769*s*, 698*m*, 657*m*, 538*w*, 521*m*. Elemental analysis calcd for $[Cu^{II}_2(\mathbf{L^1PhL^1})(Cl)_2](BF_4)_2 \cdot 2\ CH_3CN$: C 44.09, H 3.70, N 12.10; Found: C 43.18, H 3.82, N 11.80. UV-vis in CH_3CN at 0.1 mM [Cu] concentration: 260 nm (ε = 11 500 $M^{-1}\ cm^{-1}$), 310 nm (ε = 2 000 $M^{-1}\ cm^{-1}$), 380 nm (ε = 410 $M^{-1}\ cm^{-1}$), 700 nm (ε = 150 $M^{-1}\ cm^{-1}$).

*[Cu^{II}(**Py_3N**)(Cl)](BF_4)*

From **Py_3N** (160 mg; 0.55 mmol), [$Cu^{II}(H_2O)_6$](BF_4)$_2$ (96 mg; 0.28 mmol) and $Cu^{II}Cl_2 \cdot 2\ H_2O$ (47 mg; 0.28 mmol), the product [Cu^{II}(**Py_3N**)(Cl)](BF_4) (251 mg; 0.53 mmol; 96%) was obtained as a mint green powder. ESI-MS found (calculated) for [M – BF_4]$^+$ *m/z* 388.0 (388.1). IR (neat, cm^{-1}): 2974*w*, 1607*m*, 1575*w*, 1480*w*, 1438*m*, 1307*w*, 1263*w*, 1159*w*, 1113*w*, 1090*m*, 1047*vs*, 1021*s*, 958*m*, 841*w*, 771*m*, 761*s*, 643*w*, 506*m*. Elemental analysis calcd for [Cu^{II}(**Py_3N**)(Cl)](BF_4): C 43.75, H 4.08, N 11.34; Found: C 44.88, H 4.40, N 11.59. UV-vis in CH_3CN at 0.1 mM [Cu] concentration: 230 nm (ε = 7 600 M^{-1} cm^{-1}), 261 nm (ε = 12 100 M^{-1} cm^{-1}), 299 nm (ε = 3 100 M^{-1} cm^{-1}), 730 nm (ε = 90 M^{-1} cm^{-1}), 940 nm (ε = 200 M^{-1} cm^{-1}).

*[Cu^{II}(**L^{1}*SCH_3**)(Cl)](BF_4)*

From **L^{1}*SCH_3** (178 mg; 0.62 mmol), [$Cu^{II}(H_2O)_6$](BF_4)$_2$ (107 mg; 0.31 mmol) and $Cu^{II}Cl_2 \cdot 2\ H_2O$ (53 mg; 0.31 mmol), the product [Cu^{II}(**L^{1}*SCH_3**)(Cl)](BF_4) (157 mg; 0.33 mmol; 54%) was obtained as a blue powder. Crystals suitable for X-ray structure determination were obtained by slow vapor diffusion of diethyl ether into a methanol solution containing the complex. ESI-MS found (calculated) for [M – BF_4]$^+$ *m/z* 385.0 (385.0). IR (neat, cm^{-1}): 1609*m*, 1573*w*, 1483*w*, 1444*m*, 1302*w*, 1285*w*, 1160*w*, 1054*vs*, 1028*vs*, 863*w*, 820*w*, 766*s*, 652*w*, 520*m*. Elemental analysis calcd for [Cu^{II}(**L^{1}*SCH_3**)(Cl)](BF_4): C 40.61, H 4.47, N 8.88, S 6.78; Found: C 40.17, H 4.51, N 8.68, S 7.03. UV-vis in CH_3CN at 0.1 mM [Cu] concentration: 257 nm (ε = 11 000 M^{-1} cm^{-1}), 299 nm (ε = 3 600 M^{-1} cm^{-1}), 690 nm (ε = 130 M^{-1} cm^{-1}), 880 nm (ε = 160 M^{-1} cm^{-1}).

*[Cu^{II}(**$L^{2}SCH_3$**)(Cl)](BF_4)*

From **$L^{2}SCH_3$** (116 mg; 0.40 mmol), [$Cu^{II}(H_2O)_6$](BF_4)$_2$ (70 mg; 0.20 mmol) and $Cu^{II}Cl_2 \cdot 2\ H_2O$ (35 mg; 0.20 mmol), the product [Cu^{II}(**$L^{2}SCH_3$**)(Cl)](BF_4) (96 mg; 0.20 mmol; 50%) was obtained as a blue powder. Crystals suitable for X-ray structure determination were obtained by slow vapor diffusion of diethyl ether into a methanol solution containing the complex. ESI-MS found (calculated) for [M – BF_4]$^+$ *m/z* 385.0 (385.0); [M – Cl – BF_4]$^+$ *m/z* 350.0 (350.1). IR (neat, cm^{-1}): 2932*w*, 1610*m*, 1578*w*, 1460*w*, 1445*m*, 1287*w*, 1175*w*, 1050*vs*, 1026*vs*, 961*m*, 911*m*, 791*m*, 764*m*, 725*w*, 654*w*, 520*m*. Elemental analysis calcd for [Cu^{II}(**$L^{2}SCH_3$**)(Cl)](BF_4): C 40.61, H 4.47, N 8.88, S 6.78; Found: C 40.64, H 4.59, N 8.78, S 6.71. UV-vis in CH_3CN at 0.1 mM [Cu] concentration: 265 nm (ε = 10 300 M^{-1} cm^{-1}), 305 nm (ε = 3 600 M^{-1} cm^{-1}), 350 nm (ε = 2 300 M^{-1} cm^{-1}), 690 nm (ε = 320 M^{-1} cm^{-1}), 870 nm (ε = 310 M^{-1} cm^{-1}).

*[Cu^{II}(**$L^{3}SCH_3$**)(Cl)](BF_4)*

From **$L^{3}SCH_3$** (154 mg; 0.51 mmol), [$Cu^{II}(H_2O)_6$](BF_4)$_2$ (88 mg; 0.26 mmol) and $Cu^{II}Cl_2 \cdot 2\ H_2O$ (44 mg; 0.26 mmol), the product [Cu^{II}(**$L^{3}SCH_3$**)(Cl)](BF_4) (195 mg; 0.40 mmol; 78%) was obtained as a dark blue powder. Crystals suitable for X-ray structure determination were obtained by slow vapor diffusion of diethyl ether into a methanol solution containing the complex. ESI-MS found (calculated) for [M – BF_4]$^+$ *m/z* 399.0 (399.1); [M – Cl – BF_4]$^+$ *m/z* 364.0 (364.1). IR (neat, cm^{-1}): 2929*w*, 1610*m*, 1576*w*, 1474*m*, 1457*m*, 1432*w*, 1349*w*, 1287*w*, 1241*w*,

1094*m*, 1049*vs*, 1027*vs*, 964*m*, 915*w*, 803*s*, 792*m*, 773*m*, 648*w*, 520*m*. Elemental analysis calcd for [Cu^{II}(**L^3SCH_3**)(Cl)](BF_4): C 41.90, H 4.76, N 8.62, S 6.58; Found: C 42.08, H 4.73, N 8.69, S 6.52. UV-vis in CH_3CN at 0.1 mM [Cu] concentration: 267 nm (ε = 11 700 M^{-1} cm^{-1}), 319 nm (ε = 2 600 M^{-1} cm^{-1}), 358 nm (ε = 2 400 M^{-1} cm^{-1}), 650 nm (ε = 300 M^{-1} cm^{-1}), 840 nm (ε = 160 M^{-1} cm^{-1}).

*[Cu^{II}(**L^1OH**)(Cl)](BF_4)*

From **L^1OH** (194 mg; 0.80 mmol), [$Cu^{II}(H_2O)_6$](BF_4)$_2$ (138 mg; 0.40 mmol) and $Cu^{II}Cl_2 \cdot 2\ H_2O$ (68 mg; 0.40 mmol), the product [Cu^{II}(**L^1OH**)(Cl)](BF_4) (307 mg; 0.72 mmol; 90%) was obtained as a blue powder. ESI-MS found (calculated) for [M – BF_4]$^+$ *m*/*z* 341.0 (341.0). IR (neat, cm^{-1}): 3474*br*, 2949*w*, 1611*m*, 1575*w*, 1480*w*, 1443*m*, 1287*m*, 1060*vs*, 1031*vs*, 1005*s*, 983*s*, 955*m*, 871*m*, 798*s*, 763*vs*, 723*m*, 655*m*, 519*m*, 483*m*. Elemental analysis calcd for [Cu^{II}(**L^1OH**)(Cl)](BF_4): C 39.49, H 3.99, N 9.79; Found: C 39.13, H 3.97, N 9.73. UV-vis in CH_3CN at 0.1 mM [Cu] concentration: 256 nm (ε = 11 300 M^{-1} cm^{-1}), 285 nm (ε = 3 400 M^{-1} cm^{-1}), 690 nm (ε = 90 M^{-1} cm^{-1}).

*[Cu^{II}(**L^1NH_2**)(Cl)](BF_4)*

L^1NH_2 (133 mg; 0.55 mmol), [$Cu^{II}(H_2O)_6$](BF_4)$_2$ (95 mg; 0.27 mmol) and $Cu^{II}Cl_2 \cdot 2\ H_2O$ (47 mg; 0.27 mmol) were dissolved in 10 mL CH_3CN. This solution was added drop wise to 100 mL diethyl ether. The powder was filtered and washed with diethyl ether yielding [Cu^{II}(**L^1NH_2**)(Cl)](BF_4) (141 mg; 0.33 mmol; 60%) as a light blue powder. Crystals suitable for X-ray structure determination were obtained by slow vapor diffusion of diethyl ether into a CH_3CN solution containing the complex. ESI-MS found (calculated) for [M – BF_4]$^+$ *m*/*z* 340.1 (340.1). IR (neat, cm^{-1}): 3366*m*, 3303*w*, 1605*m*, 1575*w*, 1477*w*, 1447*m*, 1439*m*, 1265*w*, 1045*vs*, 1021*vs*, 964*s*, 941*m*, 886*w*, 765*vs*, 643*m*, 566*m*, 522*m*, 490*m*. Elemental analysis calcd for [Cu^{II}(**L^1NH_2**)(Cl)](BF_4): C 39.28, H 4.24, N 13.09; Found: C 39.34, H 4.27, N 12.97. UV-vis in CH_3CN at 0.1 mM [Cu] concentration: 258 nm (ε = 9 800 M^{-1} cm^{-1}), 293 nm (ε = 3 900 M^{-1} cm^{-1}), 700 nm (ε = 110 M^{-1} cm^{-1}), 690 nm (ε = 220 M^{-1} cm^{-1}).

*[Cu^{II}(**Py_2NH**)(Cl)](BF_4)*

From **Py_2NH** (223 mg; 1.12 mmol), [$Cu^{II}(H_2O)_6$](BF_4)$_2$ (193 mg; 0.56 mmol) and $Cu^{II}Cl_2 \cdot 2\ H_2O$ (96 mg; 0.56 mmol), the product [Cu^{II}(**Py_2NH**)(Cl)](BF_4) (341 mg; 0.89 mmol; 79%) was obtained as a dark blue powder. ESI-MS found (calculated) for [M – BF_4]$^+$ *m*/*z* 296.9 (297.0). IR (neat, cm^{-1}): 3466*w*, 3215*w*, 1611*m*, 1574*w*, 1483*w*, 1445*m*, 1285*w*, 1051*vs*, 1028*vs*, 1001*vs*, 935*s*, 815*w*, 764*vs*, 727*m*, 656*w*, 520*m*, 483*w*. Elemental analysis calcd for [Cu^{II}(**Py_2NH**)(Cl)](BF_4) $\cdot$ H_2O: C 35.76, H 3.75, N 10.43; Found: C 37.01, H 3.85, N 10.68. UV-vis in CH_3CN at 0.1 mM [Cu] concentration: 255 nm (ε = 12 000 M^{-1} cm^{-1}), 293 nm (ε = 2 100 M^{-1} cm^{-1}), 660 nm (ε = 120 M^{-1} cm^{-1}).

*[Cu^{II}(**Py_2S**)(Cl)](BF_4)*

From **Py_2S** (112 mg; 0.52 mmol), [$Cu^{II}(H_2O)_6$](BF_4)$_2$ (89 mg; 0.26 mmol) and $Cu^{II}Cl_2 \cdot 2\ H_2O$ (44 mg; 0.26 mmol), the product [Cu^{II}(**Py_2S**)(Cl)](BF_4) (159 mg; 0.40 mmol; 76%) was obtained as a turquoise blue powder. ESI-MS found (calculated) for [M – BF_4]$^+$ *m*/*z* 313.9 (314.0); [M + CH_3CN

– Cl – BF_4]$^+$ *m*/*z* 320.0 (320.0). IR (neat, cm^{-1}): 2929*w*, 1602*m*, 1568*w*, 1474*m*, 1446*m*, 1406*m*, 1262*m*, 1106*m*, 1074*s*, 1052*s*, 1024*s*, 997*vs*, 890*m*, 783*vs*, 764*m*, 717*m*, 649*m*, 518*m*, 475*m*. Elemental analysis calcd for [Cu^{II}(**Py_2S**)(Cl)](BF_4): C 35.84, H 3.01, N 6.97, S 7.97; Found: C 34.85, H 2.89, N 6.65, S 8.06. UV-vis in CH_3CN at 0.1 mM [Cu] concentration: 265 nm (ε = 11 600 M^{-1} cm^{-1}), 320 nm (ε = 1 900 M^{-1} cm^{-1}), 360 nm (ε = 2 800 M^{-1} cm^{-1}), 690 nm (ε = 220 M^{-1} cm^{-1}).

7.5.5 Catalysis experiments

To 1 000 μL CH_3CN in a 1 cm quartz cuvette was added 1 000 μL catalyst solution (0.0012 mmol mononuclear complex or 0.0006 mmol dinuclear complex in CH_3CN; when the complex was made in situ Na_2SO_4 was added to remove most of the H_2O present), followed by 1 000 μL 3,5-di-*tert*-butylcatechol solution (0.06 mmol in CH_3CN). The solution was stirred and kept at a temperature of 25 °C using a Cary Single Cell Peltier Accessory from Agilent Technologies (Type SPV-1X0) and a mixture of N_2:O_2(50:50) was bubbled through the solution with a needle. At the start of the measurement NEt_3 was added (8.36 μL, 0.06 mmol) and the formation of 3,5-di-*tert*-butyl-*o*-benzoquinone was monitored by measuring the absorbance at 400 nm every 0.1 sec. Every measurement was carried out in quadruplo or quintuplo. The average value is reported.

7.6 References

1. Itoh, S.; Nagagawa, M.; Fukuzumi, S., *J. Am. Chem. Soc.* **2001,** *123*, 4087-4088.
2. Ording-Wenker, E. C. M.; van der Plas, M.; Siegler, M. A.; Bonnet, S.; Bickelhaupt, F. M.; Fonseca Guerra, C.; Bouwman, E., *Inorg. Chem.* **2014,** *53*, 8494-8504.
3. Jacobson, R. R.; Tyeklar, Z.; Farooq, A.; Karlin, K. D.; Liu, S.; Zubieta, J., *J. Am. Chem. Soc.* **1988,** *110*, 3690-3692.
4. Hayashi, H.; Fujinami, S.; Nagatomo, S.; Ogo, S.; Suzuki, M.; Uehara, A.; Watanabe, Y.; Kitagawa, T., *J. Am. Chem. Soc.* **2000,** *122*, 2124-2125.
5. Kieber-Emmons, M. T.; Ginsbach, J. W.; Wick, P. K.; Lucas, H. R.; Helton, M. E.; Lucchese, B.; Suzuki, M.; Zuberbühler, A. D.; Karlin, K. D.; Solomon, E. I., *Angew. Chem. Int. Ed.* **2014,** *53*, 4935-4939.
6. Koval, I. A.; Gamez, P.; Belle, C.; Selmeczi, K.; Reedijk, J., *Chem. Soc. Rev.* **2006,** *35*, 814-840.
7. Eicken, C.; Krebs, B.; Sacchettini, J. C., *Curr. Opin. Struc. Biol.* **1999,** *9*, 677-683.
8. Allen, S. E.; Walvoord, R. R.; Padilla-Salinas, R.; Kozlowski, M. C., *Chem. Rev.* **2013,** *113*, 6234-6458.
9. Reedijk, J., *Science* **2005,** *308*, 1876-1877.
10. Ording-Wenker, E. C. M.; Siegler, M. A.; Lutz, M.; Bouwman, E., *Inorg. Chem.* **2013,** *52*, 13113-13122.
11. Ertuerk, H.; Hofmann, A.; Puchta, R.; van Eldik, R., *Dalton Trans.* **2007**, 2295-2301.
12. Turba, S.; Walter, O.; Schindler, S.; Nielsen, L. P.; Hazell, A.; McKenzie, C. J.; Lloret, F.; Cano, J.; Julve, M., *Inorg. Chem.* **2008,** *47*, 9612-9623.

13. Schindler, S.; Szalda, D. J.; Creutz, C., *Inorg. Chem.* **1992,** *31*, 2255-2264.
14. Britovsek, G. J. P.; England, J.; White, A. J. P., *Inorg. Chem.* **2005,** *44*, 8125-8134.
15. Malachowski, M. R.; Huynh, H. B.; Tomlinson, L. J.; Kelly, R. S.; Jun, J. W. F., *J. Chem. Soc., Dalton Trans.* **1995**, 31-36.
16. Ording-Wenker, E. C. M.; van der Plas, M.; Siegler, M. A.; Fonseca Guerra, C.; Bouwman, E., *Chem. Eur. J.* **2014,** *20*, 16913-16921.
17. Herges, R.; Dikmans, A.; Jana, U.; Kohler, F.; Jones, P. G.; Dix, I.; Fricke, T.; Konig, B., *Eur. J. Org. Chem.* **2002**, 3004-3014.
18. Martel, H. J. J. B.; Rasmussen, M., *Tetrahedron Lett.* **1971,** *12*, 3843-3846.
19. Sundaravel, K.; Sankaralingam, M.; Suresh, E.; Palaniandavar, M., *Dalton Trans.* **2011,** *40*, 8444-8458.
20. Tse, E. C. M.; Schilter, D.; Gray, D. L.; Rauchfuss, T. B.; Gewirth, A. A., *Inorg. Chem.* **2014,** *53*, 8505-8516.
21. Addison, A. W.; Rao, T. N.; Reedijk, J.; Vanrijn, J.; Verschoor, G. C., *J. Chem. Soc., Dalton Trans.* **1984**, 1349-1356.
22. Schatz, M.; Leibold, M.; Foxon, S. P.; Weitzer, M.; Heinemann, F. W.; Hampel, F.; Walter, O.; Schindler, S., *Dalton Trans.* **2003**, 1480-1487.
23. Winter, A.; Zabel, A.; Strauch, P., *Int. J. Mol. Sci.* **2012,** *13*, 1612-1619.
24. Solomon, E. I.; Baldwin, M. J.; Lowery, M. D., *Chem. Rev.* **1992,** *92*, 521-542.
25. Kovalchukova, O. V.; Palkina, K. K.; Strashnova, S. B.; Zaitsev, B. E., *Russ. J. Coord. Chem.* **2008,** *34*, 830-835.
26. Thomas, A. M.; Lin, B.-L.; Wasinger, E. C.; Stack, T. D. P., *J. Am. Chem. Soc.* **2013,** *135*, 18912-18919.
27. Osako, T.; Ueno, Y.; Tachi, Y.; Itoh, S., *Inorg. Chem.* **2004,** *43*, 6516-6518.
28. Midoes, A. C. D.; Aranha, P. E.; dos Santos, M. P.; Tozzo, E.; Romera, S.; Santos, R. H. d. A.; Dockal, E. R., *Polyhedron* **2008,** *27*, 59-64.
29. Monzani, E.; Quinti, L.; Perotti, A.; Casella, L.; Gullotti, M.; Randaccio, L.; Geremia, S.; Nardin, G.; Faleschini, P.; Tabbi, G., *Inorg. Chem.* **1998,** *37*, 553-562.
30. Selmeczi, K.; Reglier, M.; Giorgi, M.; Speier, G., *Coord. Chem. Rev.* **2003,** *245*, 191-201.
31. Sheldrick, G. M., *Acta Crystallogr. Sect. A* **2008,** *64*, 112-122.
32. Schreurs, A. M. M.; Xian, X.; Kroon-Batenburg, L. M. J., *J. Appl. Crystallogr.* **2010,** *43*, 70-82.
33. Sheldrick, G. M., *SADABS and TWINABS: Siemens Area Detector Absorption Correction*; Universität Göttingen: Göttingen Germany, **1999**.
34. Herbst-Irmer, R.; Sheldrick, G. M., *Acta Crystallogr. Sect. B: Struct. Sci.* **1998,** *54*, 443-449.
35. Spek, A. L., *Acta Crystallogr. Sect. D. Biol. Crystallogr.* **2009,** *65*, 148-155.